JOURNAL OF GEOPHYSICAL RESEARCH, VOL. 95, NO. A4, PAGES 3959-3985, APRIL 1, 1990

Ion Cyclotron Resonance Heated Conics: Theory and Observations

G. B. CREW, TOM CHANG, AND J. M. RETTERER[1]

Center for Space Research, Massachusetts Institute of Technology, Cambridge

W. K. PETERSON

Lockheed Palo Alto Research Laboratory, Palo Alto, California

D. A. GURNETT AND R. L. HUFF

Department of Physics and Astronomy, University of Iowa, Iowa City

A general theoretical treatment of energetic oxygen ion conic formation through cyclotron resonance with magnetospheric electromagnetic plasma turbulence is presented. With suitable assumptions, there exists a similarity regime in which the process may be profitably characterized by two parameters v_o and σ, corresponding roughly to the velocity scale and pitch angle of the ion distribution. These may be independently determined from the wave and particle observations of a conic event, as is illustrated here using typical auroral passes of the Dynamics Explorer 1 satellite. The predictions of the theory are found to be in excellent agreement with the observations.

1. INTRODUCTION

This article is concerned with a class of the energetic ion populations found within the Earth's ionosphere–magnetosphere system which are generically referred to as ion conics. The etymology of the term begins with its application to ion populations where the greatest concentration of ions lies on a cone in velocity space, but with the proliferation of both observations and theoretical models the correct application of the term has become considerably less restricted. Observationally, the term now includes a veritable zoo of ion observation events, with a variety not solely attributable to differences in instrumentation; and theoretically, there are now a number of reasonably plausible mechanisms which might be engaged to create ion populations suitable for inclusion in this zoo. The challenge to the experimentalist is to construct events sufficiently complete in their observations to allow a discrimination between theories, and the challenge to the theorist is to collect a subset of the events into a class which may be understood through the invocation of a single theory. With the aim of meeting this challenge and for the immediate goals of this paper, we are inclined to make the following definition:

Definition. An "ion cyclotron resonance heated conic," which we shall abbreviate as "ICRH conic," is an ion population of ionospheric origin which was energized primarily through an ion cyclotron resonance interaction with electromagnetic plasma turbulence. This is a resonant wave–particle interaction where the ions are extracting energy from that portion of the electric field turbulence which includes their cyclotron frequency. The result of this extraction is a net gain for the ions in their energy of motion perpendicular to the magnetic field orientation.

Unfortunately, this still results in a wide range of morphologies for the ion population, which is primarily due to the geometry in which this process takes place and the point of observation. In this paper we shall be concerned with geometries where the source of the ions lies in the ionosphere, the turbulent spectrum exists along an entire (auroral) field line, and the point of observation lies in the magnetosphere. There clearly are many other possible applications for the heating mechanism. The term "auroral" appears in parentheses because although the events we shall consider are indeed found in the auroral zone, the complete role of conics as "auroral phenomena" has yet to be fully explored. We shall return to this point later.

It is important to understand such events for a number of reasons. Among these are the fact that conics provide a release mechanism for ionospheric ions and are a major source of energetic ions for the magnetosphere. The fact that these ions have traveled up along a field line implies that they carry, to a greater or lesser extent, a signature or imprint of the plasma conditions to which they have been exposed. And we must not forget that the space environment is a useful laboratory for understanding plasma physics phenomena: here we deal with wave–particle interactions and plasma wave turbulence.

Historical overview. This is not the place to conduct an extensive general review of the growing literature on conics. Since the time of the first conic observations [*Sharp et al.*, 1977], a large number of events have been reported (see, for example, the reviews by *Klumpar* [1986] or *Burch* [1988]) and a number of theoretical models have been suggested (e.g., see the reviews by *Chang et al.* [1988] and *Lysak* [1986]). Within this larger context lies the story of ICRH conics, which begins with the observations.

Two of the observational papers are directly relevant to the present work. The event on November 14, 1981 (near 2346 UT on day 81318; for brevity the day 81318 event hereafter), reported in detail by *Winningham and Burch* [1984], presented a bit of a theoretical puzzle in that none of the previously considered wave–particle interaction mechanisms (e.g., electrostatic ion cyclotron [*Ungstrup et al.*, 1979; *Lysak et al.*, 1980; *Papadopoulos et al.*, 1980; *Dusenbury and Lyons*, 1981; *Singh et*

[1]Also at Ionospheric Physics Division, Air Force Geophysics Laboratory.

Copyright 1990 by the American Geophysical Union.

Paper number 89JA03175.
0148-0227/90/89JA-03175 $05.00

al., 1981; *Ashour-Abdalla and Okuda*, 1984, and references therein] or lower hybrid [*Chang and Coppi*, 1981; *Crew and Chang*, 1985; *Roth and Hudson*, 1985; *Retterer et al.*, 1986]) could be responsible, largely owing to the lack of the necessary waves or any means to generate them. That is, if one were to attempt an explanation of the event using electrostatic ion cyclotron waves, one would immediately founder on the lack of an electron population with sufficient free energy to generate these waves. A similar consideration applies to the possible generation of the conic via lower hybrid waves. It should also be noted that this event was presented as being typical of a large number of similar events. Although not recognized at the time, the two events (near 2045 UT on October 15, 1981, or day 81288, and near 1743 UT on March 2, 1982, or day 82061; again for brevity, the 81288 and 82061 events, respectively) simultaneously reported by *Klumpar et al.* [1984] involve similar ion distributions. However, these two were selected because of the "bimodal" nature of the distributions, which was taken as a signature of a two-stage acceleration process. That is, a low-altitude acceleration transverse to the geomagnetic field of the particles followed by acceleration along the field could account for the observations. Unfortunately, there has never been any evidence to suggest what that low-altitude acceleration process might be.

Motivated by the puzzle of the 81318 event, *Chang et al.* [1986] considered the possibility that the energization of the ions might be accomplished through cyclotron resonance in much the same fashion as heating in the ion cyclotron range of frequencies (ICRF) has been used for years in the fusion community. In this application, an antenna mounted at the surface of the plasma is used to launch electromagnetic waves which propagate into the plasma and give up a fraction of their energy to the plasma ions through cyclotron damping deep in the interior of the plasma. The analogous ionospheric–magnetospheric scenario holds some remote magnetospheric process responsible for the generation of the electromagnetic waves, which propagate to lower altitudes and dump some of their energy into the ions, providing the energy necessary for the formation of ion conics. For the 81318 event, there was no especial problem finding the waves to hold responsible for the heating, as electromagnetic turbulence in the required frequency range is a frequent occurrence on auroral field lines [*Gurnett et al.*, 1984]. In fact, not only was it a viable mechanism, but subsequent work [*Retterer et al.*, 1987*a*] was able to account not only for the energetics of the event, but for the detailed structure of the ion distribution as well. Thus the 81318 event might be considered the prototypical ICRH conic.

The similarity between the 81318 conic distribution and those of the conics reported by [*Klumpar et al.*, 1984] motivates an examination of these events within the context of the ICRH conic theory. Moreover, *Temerin* [1986], using the 81288 event as an example, pointed out that a distribution of this sort should result whenever an ion distribution is bulk heated over an extended altitude range. Indeed, granted suitable assumptions on the turbulence, preliminary work [*Retterer et al.*, 1987*b*] demonstrated that it is possible to reconstruct the form of the 81288 conic using the ICRH mechanism.

The next step, which this present work reports, is an examination of the turbulence present during these events and the convincing demonstration that the theoretical mechanism is well able to account for the details. In the process, we shall carry the comparison of theory and observations to a rather unprecedented level of detail in order to stretch the theory to its limits. The point of this paper is the establishment of ICRH conics as an observational class of events with an adequate theoretical explanation.

Organization of this paper. In the next section we delve into some of the details and specifics of the formation of ICRH conics. In the process, the physical setting is reduced to a well-posed mathematical problem. At this point we turn to a review of the particle observations and consider the wave observations. Taken together, these observations define a basis for comparison with the theory and restrict which questions may be asked and which questions answered. With this framework defined, the following section discusses solutions to the mathematical problem and lays the groundwork for the detailed comparison presented in the next section. The final section draws some conclusions from from the material presented in the paper and identifies some implications for future research.

2. ELEMENTS OF CONIC FORMATION

In this section we discuss the basic ingredients which combine to produce an ICRH conic. Since we are fundamentally concerned with a wave–particle interaction process, we will need to consider some of the details of the waves and their propagation. However, as we shall see, we will not be overly concerned with the creation and maintenance of the turbulence, so this is not a topic which merits considerable detail in the present effort. On the other hand, we are most interested in the effect of the waves on the ion population; for this we need a kinetic theory for the ions and will wish to extract from it as much information as is possible. And of course, all of this takes place within the Earth's ionosphere–magnetosphere system which imposes some considerations which we discuss first.

2.1. Global Setting

It is important to state and emphasize at the outset that we are concerned with processes which transpire along the lines of magnetic force. That is, the entire conic formation process may be viewed as taking place within a given flux tube. This is not the only geometry in which to envision the heating of ions. As noted in the introduction, the laboratory community, at the very least, has been conducting ICRF heating experiments for years. In fact, the mechanism plays an active role in equatorial regions of the magnetosphere [*Gendrin*, 1983] and recent work [*André et al.*, 1988; *Peterson et al.*, 1989] builds a fairly strong case that ICRF heating is active in the magnetospheric cusp with an altogether dissimilar geometrical setting.

The statement that ICRH conics are created entirely within a flux tube carries with it the implicit assumption that collective motion across field lines, e.g., $\mathbf{E} \times \mathbf{B}$, ∇B, etc. bulk plasma drifts, are negligible to lowest order. One could certainly include these various types of drifts as corrections; but for clarity and in the spirit of doing the zeroth-order physics first, we do not do so here in the basic treatment presented here. It is perhaps appropriate to point out here that there are treatments [*Horwitz*, 1986; *Cladis*, 1986] which consider such cross-field transport to be the main effect and look to utilization of the potential drop across the polar cap as a means of achieving particle energization. While such transport-dominated mechanisms have been proposed for the existence of a class of conics, termed "ion bowl distributions," we shall not discuss such explanations here but instead refer the interested reader to the works cited.

One of the important implications of the confinement of the process within a magnetic flux tube is that the boundary conditions on the particle motion necessary to the well-posedness

of the mathematical problem need only be applied at the ends of the flux tube. Simply put, whatever goes in at the bottom goes out at the top with no loss of ions in between. In the events under consideration, the flux of ions into the flux tube at the top (i.e., above the satellite) is negligible, thus we need not concern ourselves with particles that entered the flux tube headed down toward the Earth and through magnetic mirror or other forces are subsequently turned around to become part of the upgoing population. Thus in what follows, our task is to construct only the upward moving portion of the ion distribution function; the downward portion may be taken identically zero. For consistency in the expressions, we denote by $v_\parallel$ (>0) the upward component of ion velocity along the magnetic field, and disregard the actual orientation of the field, which changes between hemispheres.

As we shall later see, many details of source distribution function imposed at the bottom of the flux tube turn out not to be important for ICRH conics. As a preliminary consideration, we might expect it to be composed of a thermal distribution of a typical mixture of ionospheric ions. There are a number of effects which could be considered at this point which fall under the general heading of "source preparation." Given the conservation of ions in the flux tube, the density of ions at the source together with the flux-tube geometry entirely determines the density of ions observed. The upward flux of ions at the bottom by itself determines the upward flux at the satellite. Thus work showing the dependence of conic ion flux on the solar cycle [*Yau et al.*, 1988] can be understood in terms of solar cycle variations of the ionospheric source. Another case of source preparation is the notion of preheating. That is, a variety of processes (e.g., unrelated wave–particle interaction processes) might heat some components of the ambient ion population above their normal levels. This is always an issue if one wishes to discuss the relative heating/densities of conics of different species. The effects of source preparation can be incorporated merely by raising the altitude and modifying the characteristics of the source distribution. By way of summary, it might be said that the nicest feature of the geometry is that as far as the particles are concerned, all of the uncertainties are confined to the foot of the flux tube.

With regard to the waves, however, it is a different story. The most fundamental problem is the fact that the concept of a wave involves the relative motions of plasma at points separated in time and space. Given the fact that we are for the foreseeable future limited to point measurements (whether on satellite or rocket) it is clear that there are and will continue to be considerable ambiguities in the interpretation and identification of the wave data. One of the most significant problems here is the difficulty of acquiring information about the k-spectrum of the turbulence; for the present, we cannot dispense with the need for reasonable assumptions. There is also the fact that the motion of the observational platform permits the aliasing quasi-stationary structures as waves. For the most part, these are well-known, standard issues that always arise in treatments such as this [*Gurnett et al.*, 1984], and we do not have any fresh solutions. We raise the issue mostly because at some level, we reach what is essentially a fundamental assumption which the reader must either accept or reject.

An additional, related problem is that since we discuss a process that is active at all altitudes, we shall need information on the turbulence throughout the flux tube. Again, we have only the information at the satellite, along with statistical information gathered over a number of orbital passes, to guide us in the formation of reasonable models. As with the question of the source distribution, for ICRH conics this will prove not to be a difficult point. Finally, there are additional physical processes, such as the accelerating effect of a field-aligned potential drop, which one might insert at various altitudes in the flux tube. We shall find no need to include them in the present treatment.

There is a similar sampling problem in the time domain. The analysis presented in this paper has been carried out under quasi-stationary conditions. That is, the properties of the turbulence and source distribution are assumed not to vary in time, so that the conic evolution process at one instant in time looks the same as it does at a later time. The reason for this is quite simply that there is little information which can be used to supply a time variation to either of these quantities.

There are a number of preliminaries associated with the way in which the measurements are made. Recognizing that the data are acquired as a time series along the satellite trajectory, there is often a temptation to think in terms of an evolution of the ion population along the same trajectory. Instead, we must remember that the evolution of the ion distribution takes place along the flux tube. What one samples along the trajectory is a sequence of end products of the evolution process (end products as far as we shall be able to observe, that is). The variation of the observations along this trajectory is considerably more reflective of changing conditions at the source or modulations (spatial and/or temporal) in the turbulence. Aside from these imposed conditions, the evolution within a given flux tube can be considered entirely independent of that which transpires within the next. Thus if conditions require it, the data series could even be discontinuous on scale sizes larger than that of a flux tube. Of course, all of this passes through the time resolution of the specific instruments making the measurements.

2.2. *Wave Turbulence Properties*

We now give brief consideration to some of the properties of the wave turbulence present on auroral flux tubes and their effects on the heating of the ions. We are concerned with the electromagnetic turbulence in the ion cyclotron range of frequencies, which for O^+ ions ranges from a few hertz at low altitudes to less than 1 Hz at a few R_E. As we shall see below, the wave–particle interaction we consider is a resonant one: the ions have a secular response to that portion of the turbulence near their cyclotron frequency which is left-hand polarized, and they respond adiabatically to all other frequencies and polarizations. Naturally, this is a simplification, but it does indeed represent the dominant lowest-order effects.

This portion of the turbulence which is of immediate interest is immersed within the larger spectrum of electromagnetic auroral turbulence [*Gurnett et al.*, 1984]. The origin and exact nature of this turbulence is still somewhat uncertain, and to properly address these questions would go considerably beyond the scope of the present work. However, a number of the observed features are of interest. One is the fact that the electric field spectral density is typically well represented as a power law in frequency, although with varying spectral index. Additionally, the electric field spectral density was found to be relatively independent of altitude for a given frequency. Moreover, the investigation of the polarization of the electric field perpendicular to the magnetic field showed it to be essentially unpolarized for this frequency range. Finally, a conclusion from the analysis of the observations [*Gurnett et al.*, 1984] was that one could not account for turbulence entirely with static, nonpropagating spatial structures; electromagnetic wave activity was definitely present. We shall later make use of these facts to build an approximate model for

the spectrum of turbulence throughout the flux tube below the satellite, based on measurements at the satellite altitude.

Another consideration is the temporal behavior of the turbulence. We shall see that there was significant variation of the spectral power and index in the events presented. The events themselves, however, had durations on the order of minutes; considerably longer than the gyroperiod, flux tube transit time (gyroradius divided by spacecraft velocity) and at worst comparable to the duration of the heating event (i.e., transit time from lower altitudes). Unfortunately, the restrictions of a single spacecraft makes it difficult to sort out spatial and temporal effects: are these real temporal effects or merely variations from flux tube to flux tube? In the absence of definitive answers, we shall assume a quasi-steady state turbulence, and expect modification by factors of order unity should this fail to be the case.

Finally, there are the related questions of the source, maintenance, and composition of the turbulence, which go considerably beyond the scope of the the present work. *Gurnett et al.* [1984] found support for the notion that much of the turbulence could be due to Alfvén waves coupling the ionosphere to the magnetosphere [*Goertz and Boswell*, 1979; *Lysak and Dum*, 1983]; when measurable, the Poynting flux was directed earthward. On the other hand, it seems likely that no single wave mode can account for all the observations, and indeed, the various allowed plasma wave modes are probably all present to a greater or lesser degree.

On the other hand, one might conclude based on cold plasma wave theory [*Stix*, 1962] that there could be no appreciable power in left-hand polarized waves near the local ion cyclotron frequencies, as needed for the resonant wave–particle interaction. This is not a problem for several reasons [*Chang et al.*, 1986]. In a hydrogen dominated plasma, analysis of the cold plasma dispersion relation shows that the gaps in the left-hand polarized wave modes are just above the minority species cyclotron frequency, and that the width of the gap is proportional to the relative density of the minority to the majority species. For obliquely propagating modes the gap is even more narrow. On the other hand, the resonance condition is at the Doppler-shifted cyclotron frequency; i.e., offset from the gap by $k_{\|}v_{\|}$, allowing the ions to resonate with left-hand polarized waves both below and above the ion gyrofrequency [*Perkins*, 1984]. Consequently, we expect that there will be a left-hand component available for the heating of oxygen ions. These waves, however, should not be very effective in accelerating the hydrogen ions because such considerations do not apply to the majority species. In fact, for the 81318 event, the spectral density fell off at the hydrogen cyclotron frequency, providing a reasonable explanation for the fact that those conics were in oxygen.

In addition, for oblique propagation, the right-hand mode loses its pure polarization and acquires a left-hand component. Thus some of the wave power that might propagate down from higher altitudes in a right-hand polarization can be linearly mode-converted to have appreciable power in the left-hand polarization near a local cyclotron frequency [*Johnson et al.*, 1988, 1989]. Additionally, one should worry about kinetic modification of the basic cold plasma dispersion; kinetic Alfvén waves are one possibility [*Hasegawa*, 1977]. Finally, one can only begin to speculate concerning nonlinear mechanisms which might accomplish a redistribution the relative power among plasma wave polarizations and quasimodes, and in the process eliminate some the the spectral gaps expected from considerations of simple, homogeneous, linear theory. The fact that the spectral shape is typically a power law is a strong suggestion that such processes are at work. These are issues to which further attention should be given.

For the present work, we shall take the viewpoint that the plasma modes responsible for the heating represent some fraction of the total electric field spectral density observed at the local ion cyclotron frequency. Since a Doppler shift enters into the resonance condition, and there is some spread in parallel velocities for the ions, we can think of the net effect as a local frequency average performed about the cyclotron frequency. Thus we shall generally take the spectral shape to be a reasonably smooth function of frequency and not concern ourselves overly with all the irregularities of its shape. This has the effect of removing the gaps of the cold plasma theory from the explicit discussion, although as noted above, it may nevertheless be an important consideration.

Finally, it is important to note that the magnetic component of the wave activity plays no role in the heating of ions. The formulae derived in the next section to describe the heating depend only on the electric field spectral density. Magnetic measurements are important for determining the propagation characteristics of the waves, but since we shall not be dealing with this question we shall not further discuss the magnetic activity.

2.3. Heuristic Theory

The basic idea of a heuristic approach is to present the fundamental ideas in as simple a fashion as practical, recognizing that the results are probably rather approximate, but at least pedagogically valuable. Thus for the ICRH conics we follow the original derivation [*Chang et al.*, 1986] and ask what happens to a typical ion, with charge q and mass m_i, which we shall term "mean" in the sense of representing some form of average over the entire distribution of ions. We pick up the story of the mean ion adrift in a sea of plasma wave turbulence at some location l along the field line. By virtue of the notion of a resonant interaction, the ion is oblivious to all except for that fraction of wave power which is in a left-hand polarization within some narrow band about its local cyclotron frequency, $\Omega(l)$. For a brief time Δt, the ion gyrates in concert with what amounts to an effective left-hand polarized electric field $\mathbf{E}_{\perp}(l)$. The result of this dance is a change $\Delta\mathbf{v}_{\perp}$ in the ion's velocity vector $\mathbf{v}_{\perp}$ given by

$$m_i \Delta\mathbf{v}_{\perp} = q\,\mathbf{E}_{\perp}(l)\Delta t \tag{1}$$

resulting in a change in perpendicular energy

$$\begin{aligned}\Delta W_{\perp} &= \frac{1}{2}m_i(\mathbf{v}_{\perp}+\Delta\mathbf{v}_{\perp}) - \frac{1}{2}m_i|\mathbf{v}_{\perp}|^2 \\ &= m_i\mathbf{v}_{\perp}\cdot\Delta\mathbf{v}_{\perp} + \frac{1}{2}m_i|\Delta\mathbf{v}_{\perp}|^2\end{aligned} \tag{2}$$

Recalling that we really are concerned with a more or less gyrotropic distribution of ions rather than a single ion, only the last term above contributes to the rate of change due to this interaction:

$$\dot{W}_{\perp,res} \equiv \frac{\Delta W_{\perp}}{\Delta t} = \frac{q^2|E_{\perp}(l)|^2}{2m_i}\Delta t \tag{3}$$

For a broad frequency spectrum, the interaction time Δt is limited to the correlation time of the incoherent electric field which is roughly the reciprocal of the bandwidth used in defining $\mathbf{E}_{\perp}(l)$. Thus the heating rate (3) is directly proportional to the electric

field spectral energy density evaluated at the local cyclotron frequency.

At the same time, the ion is moving up the field line; its gyrofrequency changes due to the changing geomagnetic field. Thus it interacts with a band of waves centered on a different frequency, taken from a possibly different spectrum of turbulence. The expression (3) still gives the net resonant heating rate. However, at the same time as it is being heated, the mean ion is still subject to the magnetic mirror force due to the inhomogeneous geomagnetic field. In the absence of heating, this amounts to motion which preserves the ion's energy and first adiabatic invariant (its magnetic moment $W_\perp/B$). There may also be additional forces present, such as an electric field $E_\parallel = -d\phi/dl$ due to a parallel potential drop. Thus its motion may be described by equations which incorporate both of these effects [*Chang et al.*, 1986]:

$$\dot{W}_\perp = W_\perp \nu_\parallel (d \ln B/dl) + \dot{W}_{\perp,res} \tag{4}$$

$$m_i \dot{\nu}_\parallel = qE_\parallel - W_\perp (d \ln B/dl) \tag{5}$$

where $\nu_\parallel = dl/dt$. In a decreasing magnetic field geometry, the mirror force converts some of the gains in $W_\perp$ from the heating into parallel acceleration and increasing parallel energy $W_\parallel \equiv m_i \nu_\parallel^2/2$. We shall return to a solution of these equations later; for now it is enough to note that for sufficiently intense turbulence the heating dominates in equation (4) and some of the perpendicular energy gains are converted into parallel energy via equation (5). Finally, we note that heuristic equations of this sort may be constructed for virtually all conic formation mechanisms [*Chang and Coppi*, 1981; *Singh and Schunk*, 1984; *Gorney et al.*, 1985; *Singh and Hwang*, 1987].

2.4. Kinetic Formulation

Building on the material of the preceding subsections, we now turn to a precise kinetic formulation of the problem [*Retterer et al.*, 1987*a*; *Crew and Chang*, 1988*a*, *b*]. Specifically, we seek the distribution function $f(l, \nu_\parallel, \nu_\perp)$ throughout the flux tube. Here the variable l is the arclength along the magnetic field line, which corresponds roughly to the altitude. The phase space velocity variable has been decomposed into components $\nu_\parallel$ and $\nu_\perp$, parallel and perpendicular to **B**, respectively. This distribution f represents a gyrophase average of the underlying three-dimensional velocity space distribution since both the evolution of the distribution and the measurement of the complete distribution take place on time scales longer than the gyroperiod.

One route to an equation for f proceeds from the usual quasilinear equation governing the distribution in six dimensional phase space. This equation may then be averaged over the ion gyrophase (see, for example, *Crew and Chang* [1985] for more detail). Given the approximations discussed above, the evolution of the distribution takes place in the variable l:

$$\nu_\parallel \frac{\partial f}{\partial l} - \frac{q}{m_i}\frac{d\phi}{dl}\frac{\partial f}{\partial \nu_\parallel} - \frac{\nu_\perp^2}{2B}\frac{dB}{dl}\left[\frac{\partial f}{\partial \nu_\parallel} - \frac{\nu_\parallel}{\nu_\perp}\frac{\partial f}{\partial \nu_\perp}\right] = \frac{1}{\nu_\perp}\frac{\partial}{\partial \nu_\perp}\left[\nu_\perp D_\perp \frac{\partial f}{\partial \nu_\perp}\right] \tag{6}$$

The spatial variations of f are entirely controlled by the first term which follows the convective flow of ions up the magnetic flux tube, since the neglect of cross-field drifts implies the neglect of transverse gradients in f. Thus with a source distribution $f_s(\nu_\parallel, \nu_\perp)$ assigned as a lower boundary condition at $l = l_s$, we can integrate equation (6) in l to obtain the distribution at some observation point: $f_o(\nu_\parallel, \nu_\perp) \equiv f(l = l_o, \nu_\parallel, \nu_\perp)$. The next terms force the distribution to respond to the action of the adiabatic forces. As we discussed above, the presence of a gradient in the magnetic field forces the conversion of perpendicular energy to parallel energy for the bulk distribution, since the individual ions will each attempt to conserve its adiabatic invariants. Likewise a parallel electric field due to a parallel gradient in the potential $E_\parallel = -d\phi/dl$ will uniformly accelerate the ions along the field lines.

The right-hand side of equation (6) expresses the heating of ions resulting from the wave–particle interactions. The general form of the diffusion tensor for this interaction with electromagnetic waves has been worked out in some detail [*Kennel and Engelmann*, 1966]; however, for our present purposes we do not require such complexity. For long wavelengths ($k_\perp \nu_\perp$, $k_\parallel \nu_\parallel \ll \Omega$), a much simpler calculation [cf. *Sagdeev and Galeev*, 1969] results in a diffusion term of the form appearing in equation (6), with

$$D_\perp = (\pi q^2/2m_i^2) \int_0^\infty d\omega \, |E_L|^2(\omega) \, \delta(\omega - k_\parallel \nu_\parallel - \Omega(l)) \tag{7}$$

being the diffusion coefficient for ions of charge q and mass m_i expressed in terms of the electric field spectral density in left-hand polarized waves, $|E_L|^2$.

In a more general treatment the right-hand side of equation (6) would also have terms depending on other components of the diffusion tensor **D**. However, for conics the dominant effect is energization transverse to the magnetic field, which is well described by the sole term that we have retained. The Doppler shift in equation (7) is small enough that we may effectively write

$$D_\perp \simeq (\pi q^2/2m_i^2) \, |E_L|^2(\Omega(l)) \tag{8}$$

where $\Omega(l)$ is the local gyrofrequency. This results in the considerable simplification of having a velocity-independent diffusion coefficient.

An alternative, perhaps more physical, route to equation (6) recognizes that we seek a convective-diffusion equation for the density of ions per unit length of flux tube, f/B, in the coordinate space of $(l, \nu_\parallel, \nu_\perp)$. That is, the divergence of the flow due to adiabatic forces is balanced by the divergence of the flow induced by the wave–particle interactions. The components of the former are given by $\nu_\parallel$ and the parallel and perpendicular accelerations; the diffusive flow is proportional to the velocity-space gradient of f/B. Supplying values for the accelerations and diffusion coefficient, and remembering that $\nu_\perp$ is a cylindrical variable:

$$\frac{\partial}{\partial l}\left[\nu_\parallel \left[\frac{f}{B}\right]\right] + \frac{\partial}{\partial \nu_\parallel}\left[-\left[\frac{q}{m_i}\frac{d\phi}{dl} + \frac{\nu_\perp^2}{2B}\frac{dB}{dl}\right]\left[\frac{f}{B}\right]\right] + \frac{1}{\nu_\perp}\frac{\partial}{\partial \nu_\perp}\left[\nu_\perp \left[\frac{\nu_\perp \nu_\parallel}{2B}\frac{dB}{dl}\right]\left[\frac{f}{B}\right]\right] = \frac{1}{\nu_\perp}\frac{\partial}{\partial \nu_\perp}\left[\nu_\perp D_\perp \frac{\partial}{\partial \nu_\perp}\left[\frac{f}{B}\right]\right] \tag{9}$$

A slight rearrangement of terms in equation (9) reproduces equation (6).

One of the convenient features of a velocity-independent diffusion coefficient is that it becomes possible to derive from equation (9) a hierarchy of fluid equations. The fluid moments are defined as velocity space integrals:

$$\langle \nu_\perp^n \nu_\parallel^m \rangle \equiv 2\pi \int_0^\infty \nu_\perp d\nu_\perp \int_0^\infty d\nu_\parallel \, \nu_\perp^n \nu_\parallel^m \, f(l, \nu_\parallel, \nu_\perp) \tag{10}$$

Then with multiplication of equation (9) by $v_\perp^n v_\parallel^m$ and integration over the velocity space domain, one obtains

$$\frac{d}{dl}\left[\frac{<v_\perp^n v_\parallel^{m+1}>}{B}\right] + m\left[\frac{q}{Bm_i}\frac{d\phi}{dl}<v_\perp^n v_\parallel^{m-1}> + \frac{1}{2B^2}\frac{dB}{dl}<v_\perp^{n+2} v_\parallel^{m-1}>\right] - n\left[\frac{1}{2B^2}\frac{dB}{dl}<v_\perp^n v_\parallel^{m+1}>\right] = n^2\left[\frac{D_\perp}{B}<v_\perp^{n-2} v_\parallel^m>\right] \quad (11)$$

Upon rearrangement, three of these give conservation equations for the flux densities of particles ($n=0$, $m=0$),

$$\frac{d}{dl}\left[\frac{<v_\parallel>}{B}\right] = 0 \quad (12)$$

and in the absence of heating, magnetic moment ($n=2$, $m=0$),

$$\frac{d}{dl}\left[\frac{<v_\perp^2 v_\parallel>}{B^2}\right] = \frac{4D_\perp<1>}{B^2} \quad (13)$$

and energy (using equations (12) and (13) together with $n=0$, $m=2$).

$$\frac{d}{dl}\left[\frac{<v_\perp^2 v_\parallel> + <v_\parallel^3> + (2q\phi/m_i)<v_\parallel>}{B}\right] = \frac{4D_\perp<1>}{B} \quad (14)$$

As is usually the case with reduction to fluid moment equations, we do not have a closed hierarchy of equations. Thus in addition to these equations, we would need an equation for the density $n_i(l) \equiv <1>$, which would involve further moments. They can be used, however, to make global statements about the ions in the flux tube. For example, the integral of equation (14) with altitude tells how much energy the ions carry out the top of the flux tube; in a self-consistent formulation this should be balanced by the flow of energy into the flux tube for the generation and maintenance of the spectrum of turbulence.

Finally, we see that it is possible to "derive" the heuristic theory from these equations making suitable approximations to truncate the hierarchy. In particular, we can choose to define the perpendicular energy of the "mean" particle by

$$W_\perp \equiv \frac{m_i<v_\perp^2 v_\parallel>}{2<v_\parallel>} \quad (15)$$

and its upward speed by

$$v_\parallel \equiv \frac{<v_\parallel>}{<1>} \equiv \frac{dl}{dt} \quad (16)$$

Then equation (13) gives us equation (4) with a heating rate given by

$$\dot{W}_{\perp,res} = 2m_i D_\perp \quad (17)$$

The parallel acceleration of the mean particle follows from equations (12) through (14) if we further approximate

$$<v_\parallel^3> \approx \frac{<v_\parallel>^3}{<1>^2} \quad (18)$$

This last approximation is the one which renders the mean particle equations heuristic, since it is a good approximation only for relatively cold distributions.

3. OBSERVATIONS

3.1. Particle Data

The conic observations have all been previously discussed in the literature [*Winningham and Burch*, 1984; *Klumpar et al.*, 1984]; hence we shall simply summarize some of the basic facts in Table 1. The day 81318 event has already been subjected to rather extensive investigation [*Chang et al.*, 1986; *Retterer et al.*, 1987*a*], so we shall instead concentrate our detailed analysis on the other events, of which only one, the day 81288 event, has received preliminary attention [*Retterer et al.*, 1987*b*] as an ICRH conic. There is also an additional complication resulting from the fact that the 81318 event is a low-altitude, less energetic event: the distribution is well resolved only in the high altitude plasma instrument (HAPI) [*Burch et al.*, 1981] which does not have mass discrimination. While the energetic ion composition spectrometer (EICS) [*Shelley et al.*, 1981] observations do indicate that O^+ is the dominant ion species, justifying the application of the theory to the 81318 event, the EICS observations are not sufficiently resolved to merit the detailed attention we shall apply in this paper.

TABLE 1. Three O^+ ICRH Conic Events

	81288*	81318†	82061*	Units
Year	1981	1981	1982	
Day	Oct. 15	Nov. 14	Mar. 2	
UT	2046	2346	1743	h min
l_o	4.28	2.0	4.52	R_E
ILAT	73.7	60.0	66.7	degrees
MLT	811	1911	000	h min
Kp‡	3–	5	5+	
f_{ci}	0.67	5.6	0.43	Hz
$\lvert E_x\rvert^2(f_{ci})$	$\sim 1.5\times10^{-5}$	$\sim 1.2\times10^{-6}$	$\sim 8.8\times10^{-6}$	$V^2\ m^{-2}\ Hz^{-1}$
n_o	~0.3	~10	~1.4	cm^{-3}
$W_\perp$	~1020	~40	~240	eV
$W_\parallel$	~850	~30	~190	eV

Klumpar et al. [1984].
†*Winningham and Burch* [1984].
‡*Coffey* [1982*a*, *b*, *c*].

Ideally, one would like to rule out the presence of a such field-aligned potential drop, ϕ, during the event, in contrast to the suggestion of *Klumpar et al.* [1984]. We examined the local electron fluxes for one event (day 81288) using simultaneously obtained electron flux data from the HAPI instrument (J. Burch, private communication, 1987). Enhanced loss cones [*Reiff et al.*, 1988; *Collin et al.*, 1986] or shifts in the energy of peaks of photoelectron emission features [*Peterson et al.*, 1977] can be used to infer field-aligned potential drops. Unfortunately, the energy and angular resolution available set only broad limits on the range of possible field-aligned potentials below the spacecraft. The electron data are, however, consistent with no field-aligned potential. Hereafter in the analysis, we shall thus take $\phi \equiv 0$ and return to this issue in the final section of the paper.

One should note that transversely accelerated H^+ ions were also found in the 81288 and 82061 observations. For the 81288 event, they were unfortunately embedded within an energetic population, presumably of magnetospheric origin. The theory as derived does not offer a quantitative explanation for the presence of these H^+ conics, for reasons having more to do with

considerations of plasma wave modes than the wave–particle interaction itself. While it may prove possible to extend the theory to consider conic formation within the majority species, to do so would go considerably beyond the scope of the present treatment, and might also confuse the issue of the applicability of the theory as currently formulated.

The 81288 and 82061 O^+ conics are sufficiently energetic to be well resolved by the EICS instrument in the "FAST" mode in which it was operating. As indicated in the preceding section, the theoretical discussion deals with the ion distribution and moments rather than the time series of energy spectra in which the data are gathered. In order to construct a distribution function, each individual measurement (tested for significance against the noise background) was used to provide an estimate of f_o within ranges of pitch angle and velocity as determined by the angular and energy acceptances of the instrument together with the duration of the measurement. Over time, values of f_o become available for a set of points distributed on a plane in velocity space determined by the satellite rotation axis. Assuming a reasonably continuous distribution, values anywhere on the plane may be obtained through interpolation or simply reference to the nearest measured value. In the FAST mode, alternate 6-s satellite spin periods are devoted to different ion species and different (interleaved) energy acceptance ranges. Thus a partial energy scan is available after 6 s, while 18 s are required for a complete energy scan of one species.

An example of the distribution of O^+ ions obtained with the complete energy scan is presented in Figure 1, which displays the velocity distribution in the velocity plane (v_y, v_z) of measurement. A combination contour/halftone representation has been used for this and subsequent phase space plots; the darker regions correspond to the greatest phase space density and contours are logarithmically spaced at half decades. The conic is clearly visible in the lower part of the plot ($v_z < 0$ corresponds to ions drifting upward). The "boxes" in the upper part of the figure are isolated individual measurements, which due to their isolation and low count rates are of dubious significance. The conic is displayed against a uniform phase space density background for clarity. This distribution was obtained near UT 2047 (UT 74806–74824 s) on day 81288 and lies at the heart of the conic. The distribution which was displayed in Plate 2 and Figure 3 of *Klumpar et al.* [1984] was an integration over an additional six satellite spin periods' worth of oxygen data (UT 74776–74872 s), encompassing the entire event.

However, a transformation from this plane of measurement to the space of parallel and perpendicular velocity components is

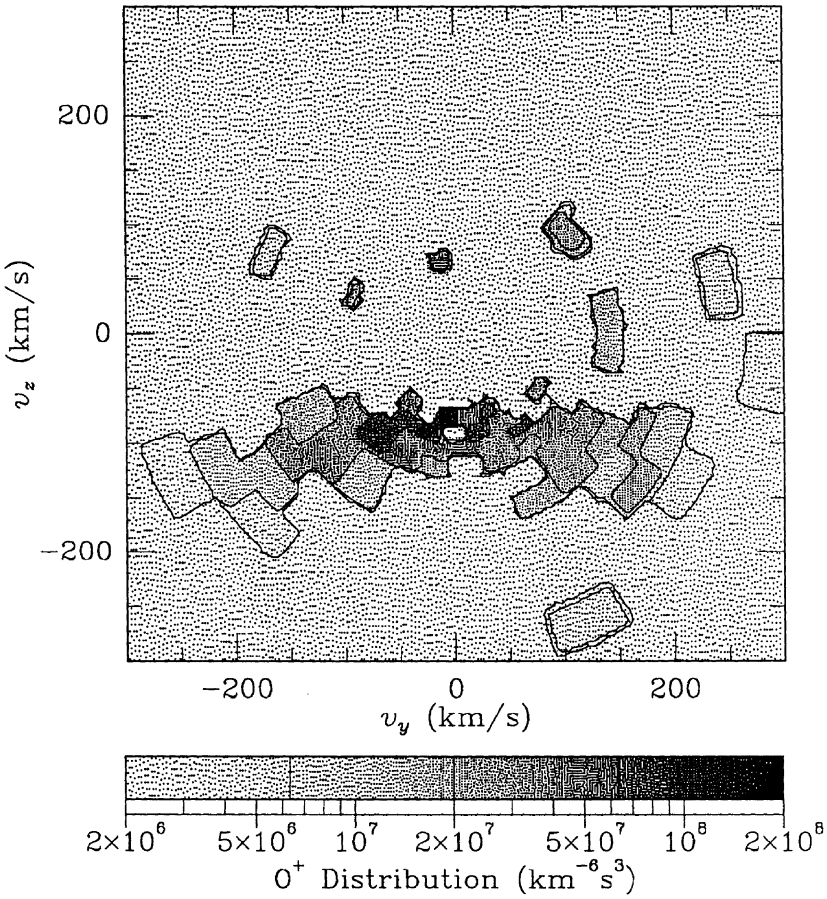

Fig. 1. Oxygen distribution function obtained during UT 74806–74824 s on day 81288. In this contour/halftone representation the darker regions correspond to the greatest phase space density and contours are logarithmically spaced at half decades.

still required. Given the relative drift between the satellite frame and the plasma frame (where it is assumed to be gyrotropic), the required transformation is easily constructed. From Figure 1 we see nothing which suggests that there are any sizeable bulk plasma drifts, so we shall simply use the satellite velocity for this relative drift. For the events considered, the plane of measurement nearly includes the field-aligned direction, so each half of this plane spans most of the $(v_\perp, v_\parallel)$ space. There are thus a variety of ways to use the data to construct $f_o(v_\perp, v_\parallel)$: the differences between them may be taken as an uncertainty of the determination of f_o, given the statistics of the measurements and other assumptions about the plasma conditions which may be only approximately satisfied. Distributions $f_o(v_\perp, v_\parallel)$ constructed from the left and right halves of Figure 1 are presented in Figures 2*a* and 2*b*. The left half (in Figure 2*a*) appears uncontaminated with ions not related to the conic per se. However, the plot does retain a certain "boxiness" which is an artifact of its construction. The notch in the distribution at $v_\perp = 0$ results from the slight misalignment (~ 2°) between the plane of measurement and the magnetic field. This artifact of the data processing is of no consequence in the subsequent analysis. Another artifact worthy of mention at this point is the fact that the lowest energy bin of the EICS instrument samples all O^+ ions with velocities $v \lesssim 40$ km/s in these plots. Now, the EICS count rate is proportional to the flux divided by energy (i.e., velocity squared). This means that we cannot calculate O^+ velocity space densities below 40 km/s.

3.2. Wave Data

The oxygen cyclotron frequency range is sampled at low and intermediate altitudes by the low frequency correlator (LFC) of the plasma wave instrument (PWI) [*Shawhan et al.*, 1981]. At the highest altitudes where the cyclotron frequency is lower, however, one must obtain the spectral data from the dc electric field portion (DC) of the PWI. In either case, we need to construct from the observed electric field spectrum a model for the left-hand polarized component along the entire flux tube. Since the LFC observations were generally found not to vary significantly with altitude [*Gurnett et al.*, 1984], we assume that this is also the case for the spectrum we shall construct from the DC data.

Both the LFC and DC measurements are of an electric field E_x

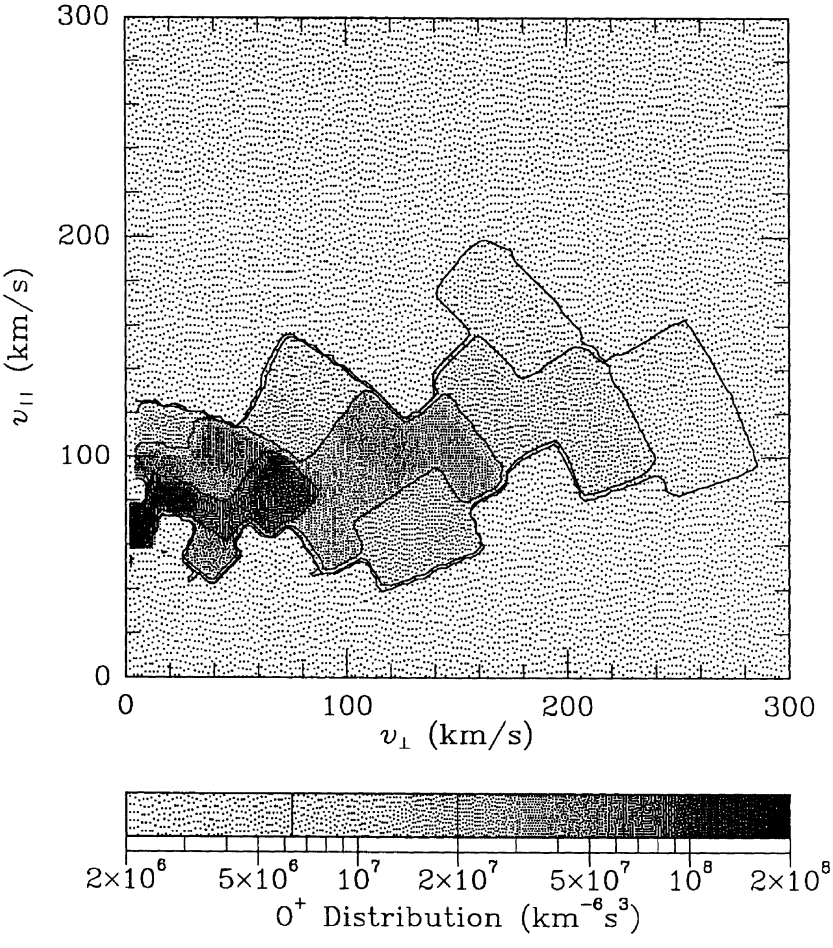

Fig. 2. (*a*) Conic distribution $f_o(v_\perp, v_\parallel)$ constructed from the left half of Figure 1, with contours at half decades and the darker regions denoting greatest phase space density.

along the satellite x direction, which rotates in a plane roughly including the magnetic field. For the LFC spectral data, which is integrated over 32 s, this provides some form of average over parallel and perpendicular polarization components of the electric field turbulence. With the DC data, one might hope to do better, but unfortunately, the satellite spins fast enough relative to the cyclotron frequency that it is not practical to do anything other than treat the spectra obtained as a similar polarization average. Thus we are forced to represent the electric field spectral density in the left-hand polarization as an undetermined fraction η of the observed spectral density: $|E_L|^2 \sim \eta|E_x|^2$. At frequencies greater than the satellite spin frequency, where the frequency shifts due to the modulation of the electric field signal by the satellite spin can be neglected, we can write $|E_x|^2 \simeq [|E_\parallel|^2 + \varepsilon|E_L|^2 + (1-\varepsilon)|E_R|^2]/2$, where $|E_\parallel|^2$, $|E_L|^2$ and $|E_R|^2$ are the spectral densities of the electric field polarizations parallel and perpendicular to B, respectively. Thus for example, we see that a value of $\eta \sim 1$ with $\varepsilon \sim 1/2$ corresponds to unpolarized turbulence (i.e., equal amounts of the parallel and two perpendicular polarizations). The question of agreement between theory and experiment can then be phrased in terms of the plausibility of the required values of η.

A portion of the DC data for the event on day 81288 are shown in Figure 3. Each frame of this figure shows E_x measured in millivolts per meter as a function of time during one spin of the satellite (6 s). For this illustration, a constant offset in the electric field and the projection onto the antenna direction of a constant electric field have been determined by linear least squares fitting for each spin and have been subtracted from the data. The antenna is aligned (as closely as possible) with the geomagnetic field at the start of each frame. Thus the relative nulls in the electric field fluctuations at the beginning, the midpoint, and the end of each frame indicate that the amplitude of the parallel electric field fluctuations is quite a bit smaller than the amplitude of the perpendicular field fluctuations. As mentioned above, however, the relative speed of the satellite spin compared to the oxygen gyrofrequency makes it difficult to estimate quantitatively the separate amplitudes of the parallel and perpendicular polarizations in that frequency range. However, from Figure 3 (and similar plots for the 82061 event) we see that $|E_\parallel|^2 \ll \varepsilon|E_L|^2 + (1-\varepsilon)|E_R|^2$, so that equal intensities of the perpendicular polarizations ($\varepsilon = 1/2$) corresponds to $\eta \sim 2$.

As an alternative to the standard fast Fourier transform (FFT) algorithm for obtaining the spectra from the DC electric field values, we have made use of the maximum entropy method

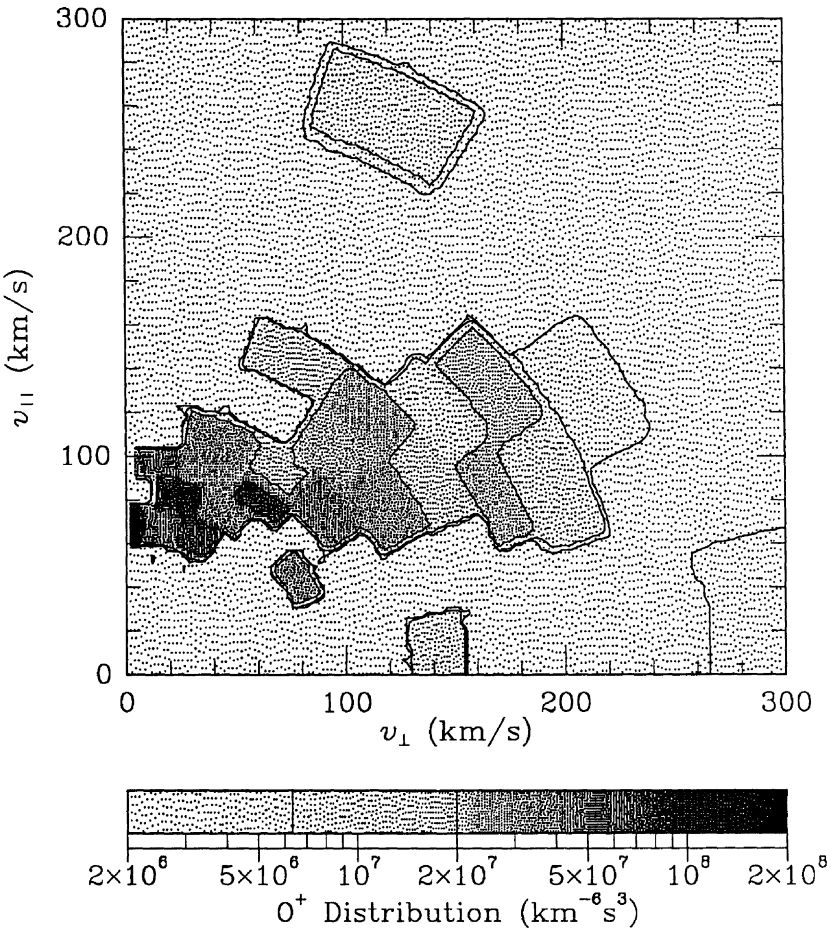

Fig. 2. (*b*) Conic distribution $f_o(v_\perp, v_\parallel)$ constructed from the right half of Figure 1, in the same format as Figure 2*a*.

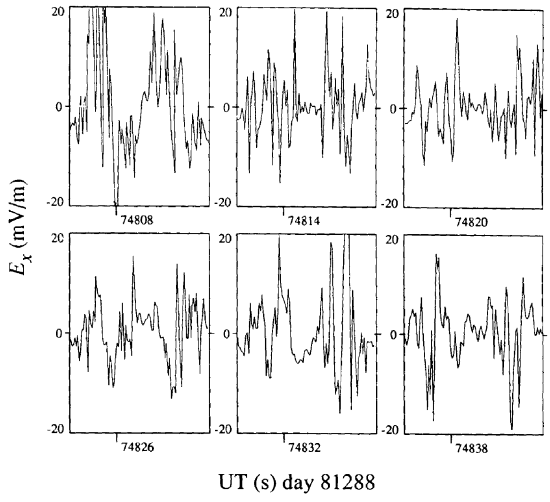

Fig. 3. Electric field data from the PWI DC field instrument for six satellite spins during the event on day 81288. Each frame shows the electric field in millivolts per meter as a function of time in seconds during one spin of the satellite.

(MEM) [*Press et al.*, 1986]. In addition to its well-known ability to resolve sharp spectral features, it tends to do a better job representing smooth, power law spectra of the type observed [*Fougere*, 1985]. In particular, we have used a 20-pole approximation to determine the spectrum for each DE-1 spin period (6 s) and evaluated the result over intervals of frequency corresponding to an FFT of one-half spin (1/3 Hz) for frequencies between the local cyclotron frequency (~ 1/2 Hz). and the Nyquist frequency (8 Hz). The results are compared with the LFC data near 2047 UT in Figures 4*a* and 4*b*. Each figure contains three spectra of DC data within the 32-s integration period of the LFC. Although there is considerable spin to spin variability in the DC spectrum, the envelope is consistent with the trend of the LFC spectrum. This is emphasized by the power law fit to the DC spectrum, which appears in each plot as a dashed line, and which lines up with the LFC trend. It should also be noted that the MEM produces results which are less "noisy" than their corresponding FFT counterparts.

While a variability is discernible between Figures 4*a* and 4*b*, the temporal flow of the event is not obvious. To capture this we turn to Figure 5 which plots the DC spectra in a time series format, plotting the electric field spectral density in a combination contour/halftone representation. What is immediately obvious from the figure is that the peak of wave activity occurs near the center of the figure (~ UT 74800 s). This is in some respects analogous to the sequence observed in the energy-time spectra of the EICS data (left-hand side of the top panel Plate 1 of *Klumpar et al.* [1984]). After we have examined the theoretical analysis in more detail in the next section, we shall be able to demonstrate a time correlation in section 5.

4. Theoretical Developments

There are a number of avenues which lead to a solution of the conic formation problem as outlined in section 2. We shall discuss each in turn.

4.1. Monte Carlo Solution

A fairly direct approach is to make use of the Monte Carlo solution technique, which was first applied to the formation of lower hybrid conics [*Retterer et al.*, 1983]. The idea here is to

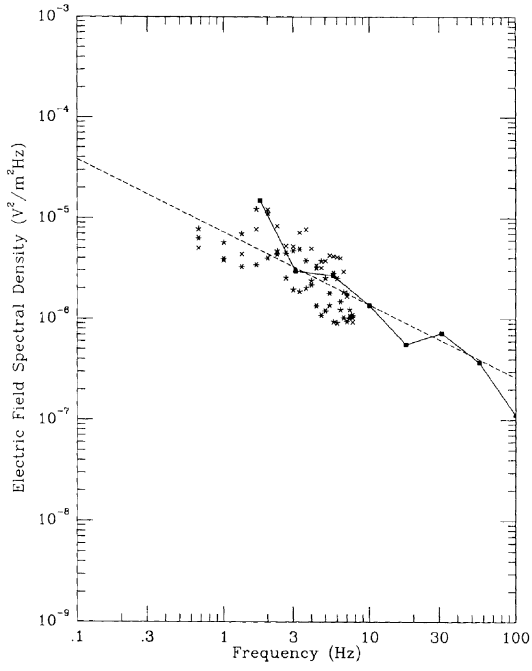

Fig. 4. (*a*) Electric field spectral density before 2047 UT on day 81288. The LFC spectrum is the solid line connecting solid squares and was taken during UT 74796–74828 s. The DC spectra are presented as 4-, 5-, and 6-pointed stars for spins beginning at UT 74808, 74814, and 74820 s, respectively. The dashed line is a power law fit to the three DC spectra with slope $\alpha \sim 0.72$.

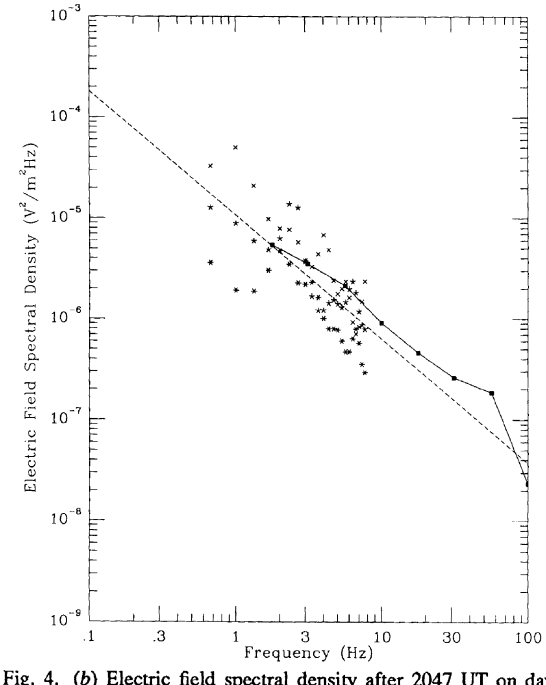

Fig. 4. (*b*) Electric field spectral density after 2047 UT on day 81288. The LFC spectrum is the solid line connecting solid squares and was taken during UT 74828–74860 s. The DC spectra are presented as 4-, 5-, and 6-pointed stars for spins beginning at UT 74826, 74832, and 74838 s, respectively. The dashed line is a power law fit to the three DC spectra with slope $\alpha \sim 1.2$.

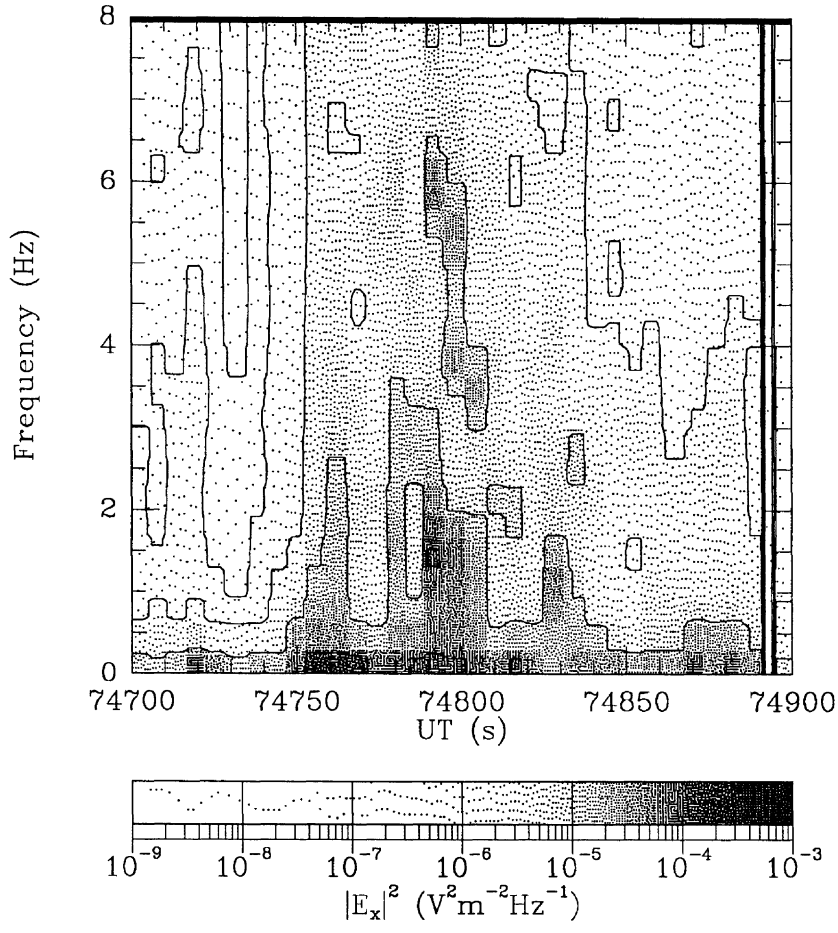

Fig. 5. Electric field spectral density based on the DC data plotted as a function of UT on day 81288. A contour/halftone format is used, where the contours are logarithmically spaced by decades, and the darker regions correspond to the greater spectral density. There is a data gap near UT 74900 s.

follow some number of "test" particles through their journey up the flux tube. The action of the wave turbulence is mimicked by the application of a sequence of random velocity kicks Δv which result in velocity space diffusion. An observed spectrum of turbulence may be invoked to determine the strength of the diffusion via equation (8); the principle uncertainties here are the fractional polarization parameter η and the exact form of the initial distribution. A suitable value for η may be obtained by integrating the heuristic equations (4) and (5) and comparing the resulting conic energy with the observed values.

The results of applying this technique to the day 81318 event are shown in Figure 6 [*Retterer et al.*, 1987*a*]. The electric field spectral density was taken to be a power law function of frequency with spectral index α:

$$|E_L|^2(\omega) \propto \omega^{-\alpha} \tag{19}$$

Now the cyclotron frequency varies with the magnetic field which in turn varies roughly with l as $(l/l_o)^{-3}$,

$$\Omega(l) \equiv (q/m_i c)B(l) \propto (l/l_o)^{-3} \tag{20}$$

so the diffusion coefficient varies with altitude as

$$D_\perp \approx D_o(l/l_o)^{3\alpha} \tag{21}$$

Using equation (8) the scaling coefficient D_o is then given in SI units by

$$D_o \approx (\eta q^2/4m^2)|E_x|^2(f_{ci}) \tag{22}$$

where $f_{ci} \equiv \Omega(l_o)/2\pi$ is the local cyclotron frequency in hertz. [Equation (22) includes a factor 2π for conversion of the frequency domain from s^{-1} to the conventional hertz.] The simulation used a spectral index $\alpha = 1.7$ and intensity $|E_x|^2 = 1.2\times10^{-6}$ $V^2\,m^{-2}\,Hz^{-1}$ at $f_{ci} = 5.6$ Hz, derived from the simultaneous LFC measurements. The mean particle calculations [*Chang et al.*, 1986] indicated a value of $\eta \sim 1/8$ was appropriate. The temperature of the initial distribution was taken ~ 0.2 eV, which is appropriate for O^+ ions at 1.2 R_E geocentric. No field-aligned potential drop ($\phi \equiv 0$) was required to produce the net upward drift of the conic.

One of the interesting results of the simulation (aside from the excellent agreement) is the insensitivity of the result to the initial distribution. Basically, the cooperative action of the diffusion and mirror forces is sufficiently strong to rapidly rearrange the initial form of f into that of a conic. Indeed, in the simulation, the ion distribution was recognizably a conic after only a several hundred km increase in altitude. Thereafter, the form of the distribution

remained relatively fixed while becoming more energetic with increasing altitude. This sort of evolution is termed self-similar, and is illustrated in Figure 7. The sequence of distributions appearing in the left panels of Figure 7 were constructed at 2.0, 1.9, and 1.5 R_E. At the lowest altitude shown, the distribution is clearly still evolving from its initial form, but is nevertheless recognizably a conic. At the highest altitudes, the shape of the conic appears fixed; the distribution is only becoming more energetic with increasing altitude. The right-hand panels are the same distributions subjected to a similarity velocity variable transformation which will be discussed in the next section. Its effect, however, is to render the three right-hand panels nearly identical.

In retrospect, there was an indication in the original discussion of the heuristic theory [*Chang et al.*, 1986] that this should be the expected behavior. There it was found that with increasing altitude, the mean particle approached a constant pitch angle, $\arctan[(6\alpha + 2)^{1/2}/3]$, while increasing continuously in energy. In fact the dependence of the total mean particle energy on l could be expressed [*Retterer et al.*, 1987*a*]

$$W_\perp + W_\parallel = \frac{(3\alpha + 11/2)^{1/3}}{(3\alpha + 1)^{2/3}} m_i (l D_\perp)^{2/3} \qquad (23)$$

which is a power law in altitude. Since the only remnant of the conic's shape preserved by the mean particle representation is its pitch angle, these results are seen to be consistent. The underlying explanation for the self-similar evolution is the fact that the magnetic field and diffusion coefficients are both roughly power law functions of altitude. The former is due to the Earth's magnetic field being roughly dipolar at these altitudes. The latter is a consequence of the power law dependence of the observed turbulence on frequency, equation (19), and the use of this observed spectrum to represent the turbulence at all altitudes, as implied by the observations as discussed above in section 2.2. In the next section we shall explore this self-similar evolution in more detail.

4.2. Similarity Regime

The essential point we shall exploit here is the fact that the high-altitude conic observations are made in this similarity regime where the conic evolution is self-similar. That is, the observations are made above the altitudes where the distribution is in the process of relaxing onto the conic shape and still retains some of its initial character. This gives us the freedom to ignore details of the initial (unknown) distribution f_s because they are irrelevant. The situation is entirely analogous to the process of striking a tuning fork to produce a tone. After a brief interval, one obtains the same tone, independent of how the tuning fork was struck.

4.2.1. Velocity scaling. We have seen how this regime is achieved by the mean particle: its energy increases as a power law with altitude. More generally, we could turn to the moment equations (11) and consider solutions where the moments vary as l/l_o to some power. Using a dimensional analysis, suppose that each factor of velocity brings to the moment an additional factor $(l/l_o)^\sigma$, where σ is a scaling parameter. Then using the expression (21) for $D_\perp$, the left and right sides of equation (11) scale with (l/l_o) in the same way only for

$$\sigma \equiv \frac{3\alpha + 1}{3} \qquad (24)$$

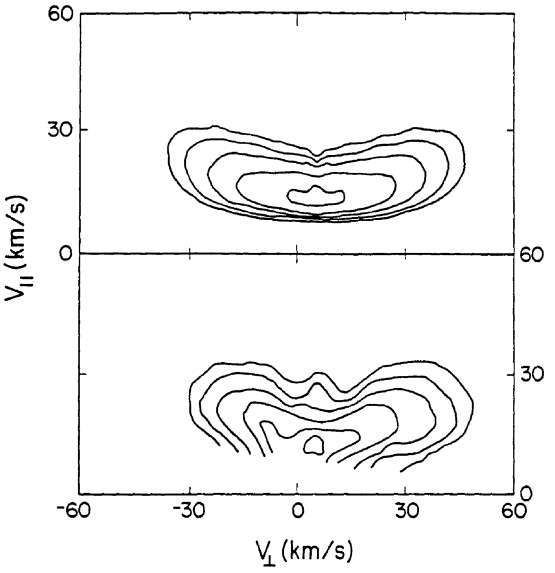

Fig. 6. The top panel is the result of a Monte Carlo calculation for the day 81318 oxygen-dominated conic obtained with the HAPI instrument which is displayed in the bottom panel. The contours in both panels are uniformly spaced with an increment of 0.4 in the logarithm of the phase space density.

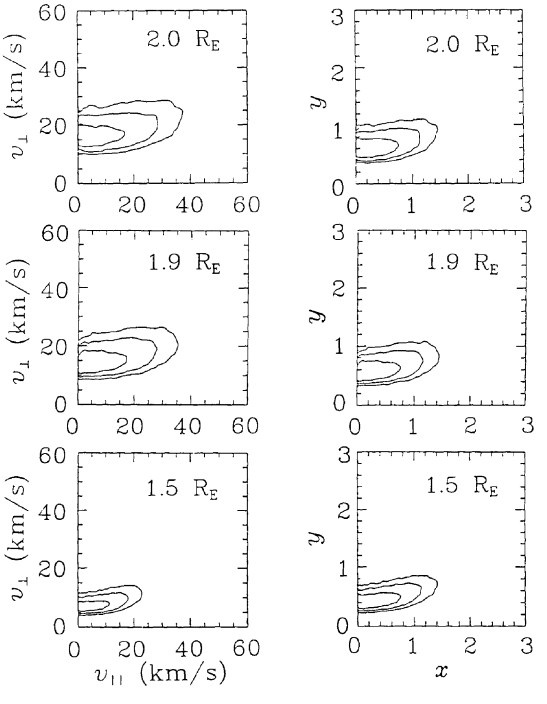

Fig. 7. The left panels present a sequence of conics constructed at the intermediate altitudes $\alpha \sim 1.2$ in the Monte Carlo simulation for the day 81318 conic shown in Figure 6. The contours here are at half decades of phase space density. The right panels are the same distributions with the velocity scales plotted in terms of the similarity variables x and y discussed in section 4.2.

(This is the same scaling as for the mean particle energy (23), i.e., $W_\perp + W_\parallel \propto (l/l_o)^{2\sigma}$.) The imposition of particle conservation on the flux tube (via equation (12)) then requires the individual moments to scale as

$$< v_\perp^n v_\parallel^m > \propto (l/l_o)^{(n+m-1)\sigma - 3} \tag{25}$$

in the similarity regime. One immediate consequence of this is that the density

$$n_i(l) \equiv < 1 > \propto (l/l_o)^{-(\sigma+3)} \tag{26}$$

i.e., the density of the conic decreases with altitude faster than the flux density, which is consistent with the upward acceleration of the ions.

This velocity scaling converts equation (11) into a three-term recursion relation among the moments of the distribution:

$$3m < v_\perp^{n+2} v_\parallel^{m-1} > - [n(3+2\sigma)+2m\sigma] < v_\perp^n v_\parallel^{m+1} > + 2n^2 v_o^3 < v_\perp^{n-2} v_\parallel^m > = 0 \tag{27}$$

where $v_o \equiv (D_o l_o)^{1/3}$ follows from the use of expression (21). Thus, for example, with $n = 0$ and $m = 1$ we find

$$\frac{< v_\perp^2 >}{< v_\parallel^2 >} = \frac{2\sigma}{3} \tag{28}$$

which gives the same pitch angle toward which the mean particle relaxes. Of course, equation (27) gives relations among an infinite set of moments, not just the lowest-order ones. Moreover, the relations are entirely determined by the two parameters σ and v_o. Unfortunately, the moments themselves are still undetermined, since one may assign arbitrary values to an infinite subset of the moments and still satisfy relation (27).

4.2.2. Kinetic equation. Another use for the similarity scaling is to transform the altitudinal evolution out of the kinetic equation. To this end, it is convenient to introduce a pair of similarity variables x and y corresponding to the perpendicular and parallel components of velocity, respectively [*Crew and Chang*, 1988*a*]:

$$x(v_\perp, l) \equiv (v_\perp/v_o)(l/l_o)^{-\sigma} \tag{29a}$$

$$y(v_\parallel, l) \equiv (v_\parallel/v_o)(l/l_o)^{-\sigma} \tag{29b}$$

The shape of the conic is then given by a dimensionless distribution $F(x, y)$ related to $f(l, v_\parallel, v_\perp)$ by

$$f(l, v_\parallel, v_\perp) = n_i(l_o) v_o^{-3} F(x(v_\perp, l), y(v_\parallel, l)) (l/l_o)^{-(4\sigma+3)} \tag{30}$$

in the similarity regime. The last factor is the scaling that guarantees equation (25) and in particular ensures the conservation of ions in the flux tube. The scaled distribution $F(x, y)$ calculated using $f(l, v_\parallel, v_\perp)$ from the left-hand column of Figure 7 is plotted in the right-hand column of Figure 7. In particular, in the upper two right-hand panels, the distributions are identical, so this procedure is clearly correct. At the lowest altitude plotted, as we indicated above, there has been insufficient evolution of the conic, and the similarity distribution is only an approximate representation for the conic.

The equation which determines F may be usefully cast as a convective-diffusion equation for a density $N(x, y) \equiv x\, F(x, y)$:

$$\nabla\cdot(\mathbf{u}N) = \frac{\partial^2 N}{\partial x^2} \tag{31}$$

with an imposed flow field

$$u_x \equiv \frac{1}{x} - \left[\frac{3}{2} + \sigma\right] x y \tag{32a}$$

$$u_y \equiv \frac{3}{2}x^2 - \sigma y^2 \tag{32b}$$

This flow results from the combined effects of the magnetic mirror force, the mean particle heating, and the scaling of velocities. The random component of the diffusion process is described by the right-hand side of equation (31).

The Monte Carlo approach may be applied effectively to the solution of this equation [*Crew and Chang*, 1988*a*]. The central idea is to treat equation (31) as the time-asymptotic limit of a Fokker–Planck equation. One may then launch a single particle and follow its evolution according to Langevin equations. The distribution $N(x, y)$ is then available as the time integral of the particle distribution divided by the duration of the simulation. From $N(x, y)$ we may construct $F(x, y)$ through division by x. This procedure is considerably more efficient than the more general Monte Carlo procedure discussed above, which must retain all of the details of the altitudinal evolution. We shall use this procedure to determine conic distributions for comparison with the observations in section 5.

4.2.3. Path integral results. Further progress can be made with the theory in the similarity regime. We have seen that while the moments of the conic are related through the recursion relation (27), they remain undetermined. In the preceding subsection, we have discussed a numerical technique which may be used to construct the distribution function F; moments can be constructed from it through velocity space integrations. However, if moments are the immediate goal, we can proceed directly to their evaluation by means of a path integral technique [*Crew and Chang*, 1988*b*].

The details are beyond the scope of this paper. However, the basic idea is that a probability density functional P is available to assign relative probabilities to any path $\Psi(t)$ the ion might take in obeying the Langevin equations for a single particle which may be derived from the kinetic equation. Expressed as a functional of position (x, y) and conjugate momenta (p_x, p_y) components of Ψ,

$$P[\Psi] = \exp\left\{ i \int dt \left[p_x(u_x - \dot{x}) + p_y(u_y - \dot{y}) + i p_x^2 x \right] \right\} \tag{33}$$

Arbitrary moments $M(\Psi)$ of the distribution may then be constructed as weighted path integrals:

$$< M(\Psi) > = \frac{\int D\Psi\, M(\Psi)\, P[\Psi]}{\int D\Psi\, P[\Psi]} \tag{34}$$

It turns out that evaluation of these moments is practical via a Feynman diagram perturbation expansion technique. The unperturbed system corresponds to an ion oscillating about the fixed point of the flow $\mathbf{u}$. The effective perturbation parameter is the relaxation time for the ion to return to this fixed point; this time decreases with increasing σ. It is then practical to obtain arbitrary moments of the conic by algebraic means.

Results of the calculation for the parallel ($n_i v_o^2 < x^0 y^2 >$) and perpendicular ($n_i v_o^2 < x^2 y^0 >$) energy densities, and the parallel ($n_i v_o^3 < x^0 y^3 >$) and perpendicular ($n_i v_o^3 < x^2 y^1 >$) energy flux densities are shown in Figure 8. While the parallel quantities vary with σ by over an order of magnitude for the range plotted, the

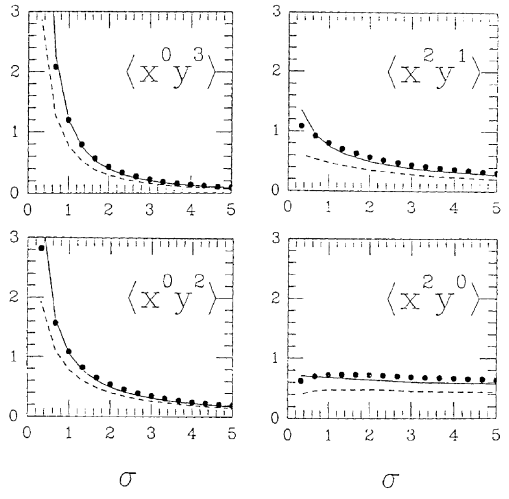

Fig. 8. Results of the path integral calculation for the parallel ($n_i v_o^2 < x^0 y^2 >$) and perpendicular ($n_i v_o^2 < x^2 y^0 >$) energy densities, and the parallel ($n_i v_o^3 < x^0 y^3 >$) and perpendicular ($n_i v_o^3 < x^2 y^1 >$) energy flux densities. The solid circles correspond to numerical similarity regime solutions. The dashed and solid curves are the result of the zeroth and first order of perturbation theory, respectively.

perpendicular quantities are relatively insensitive to σ. This is due to the fact that smaller values of σ correspond to effectively larger parallel drifts, while at the same time the relative strength of the diffusion is roughly independent of σ. The solid circles correspond to numerical solutions of the kinetic equation (31). The zeroth and first order of the perturbation expansion are indicated by dashed and solid curves, respectively.

A number of features are worthy of note. One is the fact that the expansion improves with increasing σ. This is due to the fact that at large σ particles are more rapidly swept into the sink of the flow **u**. The result is a comparatively tighter conic. Conversely, as σ decreases, the turbulence is able to better scatter the ions against this flow, resulting in a greater dispersal of ions in phase space; a distribution that might appear to be a "heated beam" rather than a conic.

The energy density moments may be compared with the heuristic result for the mean particle energy. For comparison with the path integral results we rewrite equation (23):

$$W_\perp + W_\parallel = \frac{m_i v_o^2}{2} \left(\frac{l}{l_o}\right)^{2\sigma} \left[\left(\frac{2}{3\sigma}\right)^{2/3} (6\sigma + 9)^{1/3}\right] \qquad (35a)$$

$$\approx \frac{m_i v_o^2}{2} \left(\frac{l}{l_o}\right)^{2\sigma} \left[< x^2 y^0 > + < x^2 y^1 >\right] \qquad (35b)$$

Comparison of the numerical values of the factors in brackets places the heuristic result (35*a*) in excess of the path integral result (35*b*) by about 2–7%.

A final point to note is that the results are not terribly sensitive to σ. One could interpret this to mean that formation of a conic is relatively insensitive to the spectral index of the applied turbulence. Alternatively, a determination of the spectral index from the moments of the conic distribution is not likely to be an accurate procedure. On the other hand, the moments nevertheless contain substantial information concerning the particle distribution and indeed could be used to categorize particle observations, e.g., as an extension of the current use of densities, drifts and temperatures.

5. Agreement With Observations

5.1. Preliminaries

With this theoretical groundwork laid, we are now in a position to delve into the details of the two EICS events and compare the model predictions with these data. One way to view the approach of this section is to recognize that the EICS and PWI instruments are making measurements of a priori unrelated plasma phenomena. A wave–particle interaction theory then makes some statements about how these measurements might be related. For the ICRH conic theory, the statements concerning their relationship are quantitative.

There are two aspects of this correlation which we shall consider here. One is the consideration that the PWI measures turbulence which the theory says should produce a conic of a particular form. Thus we shall compare the conic observed by the EICS with a similarity regime solution of equation (31). Second, these events exhibit some temporal variation along the DE-1 trajectory, which reflects changing conditions from flux tube to flux tube. Thus we would expect variations in the conic to track variations in the turbulence. Since it is difficult to follow a time series of distribution functions, we shall make use of moments of the conic to demonstrate this effect.

As we have seen in the preceding section, the properties of the similarity regime solutions are entirely characterized by the two parameters σ and v_o. Both of these parameters can be determined independently from each of the instruments. Thus from the PWI observations, we compute σ from the spectral index α via equation (24) and obtain $v_o \equiv (D_o l_o)^{1/3}$ from expression (22). For O^+ ions, we obtain the convenient formula:

$$v_o \equiv 38.52 \left[\frac{l_o}{1\ R_E}\right]^{1/3} \left[\frac{\eta |E_x|^2 (f_{ci})}{10^{-6}\ \mathrm{V^2\ m^{-2}\ Hz^{-1}}}\right]^{1/3} \text{(km/s)} \qquad (36)$$

To determine these parameters from the EICS observation of f_o, we note that each instance of the recursion relation (27) presents us with a linear relation in σ and v_o. Any two of these relations may be solved to yield their values, but we would not expect different pairs to result in the same values unless f_o is truly an ICRH conic and all the approximations are applicable. In practice, we obtain σ and v_o from a least squares fit to the three relations given in Table 2. Some appreciation of the relative error involved may be obtained by considering the spread of the solutions to these relations taken pairwise.

TABLE 2. Moment Relations for σ and v_o

n	m	$(\cdots)\ \sigma -$	$(\cdots)\ v_o^3 =$	$(\cdots)$
0	1	$(2 < v_\parallel^2 >)\ \sigma -$	$(0)\ v_o^3 =$	$(3 < v_\perp^2 >)$
2	0	$(4 < v_\perp^2 v_\parallel >)\ \sigma -$	$(8 < 1 >)\ v_o^3 =$	$(-6 < v_\perp^2 v_\parallel >)$
2	1	$(6 < v_\perp^2 v_\parallel^2 >)\ \sigma -$	$(8 < v_\parallel >)\ v_o^3 =$	$(3 < v_\perp^4 > - 6 < v_\perp^2 v_\parallel^2 >)$

5.2. Day 81288

We have already discussed some of the particulars of this event while describing the data reduction in section 3. Thus we first address the extent to which the conic observed is consistent with

the form predicted by theory. We would expect to see the most energetic, and therefore best resolved, conic near the peak of the event determined from the wave activity (UT 74800 s from Figure 5). We also note from Figures 1, 2*a* and 2*b*, that the number of significant counts in one complete energy scan is somewhat marginal for determining the conic structure. Thus we average the results of three complete energy scans (UT 74794–74836 s) and present the results in Figure 9*a*.

For comparison with the numerical solutions for $F(x, y)$, we compute the moments of this distribution, finding a density $n_i(l_o) \approx 0.3$ cm^{-3}, $v_o \approx 162 \pm 5$ km/s, and $\sigma \approx 2.76 \pm 0.2$. Thus (in round figures) we apply a velocity scale $v_o = 160$ km/s to the numerical solution obtained with $\sigma = 8/3$ and present the result in Figure 9*b*. Allowing for the artifacts of the data acquisition and reduction, the agreement between Figures 9*a* and 9*b* is remarkable: both distributions peak near $v_\parallel \sim 80$ km/s as $v_\perp \to 0$, and the $v_\perp$ extent of the contours is comparable. There are several measurements in the observational plot (e.g., for $v_\perp \sim 300$ km/s) which have no counterpart in the theoretical distribution; these are probably part of an unrelated oxygen population.

Given this agreement, we next turn to the time series of the observations. A determination of v_o and σ from the EICS observations can be made on a spin by spin basis; the result is presented in Figure 10*a*. Two 6-s spin periods separated by a spin period (or a total of 18 s) are required to construct a complete O^+ energy distribution which includes left and right halves; thus Figure 10*a* expresses the results obtained by various ways in order to express some of the uncertainties inherent in this calculation. In particular, there are dotted and dashed lines, which correspond to the right and left halves of the conic, respectively, and these traces are doubled because there are two ways to pair adjacent spins. The sum of the left and right halves is plotted as points (squares and triangles denoting the pairing of spins), with vertical error bars based on the uncertainty in the determination of v_o and σ as described above and horizontal error bars indicating the interval of measurement (18 s).

An immediate impression from Figure 10*a* is that the determination of σ is not nearly as precise as that of v_o. This shows up in the error bars as well as the general scatter of the data points. The primary explanation for this is the fact that although σ determines the shape of the conic, its control is somewhat subtle. While there is considerable qualitative difference between

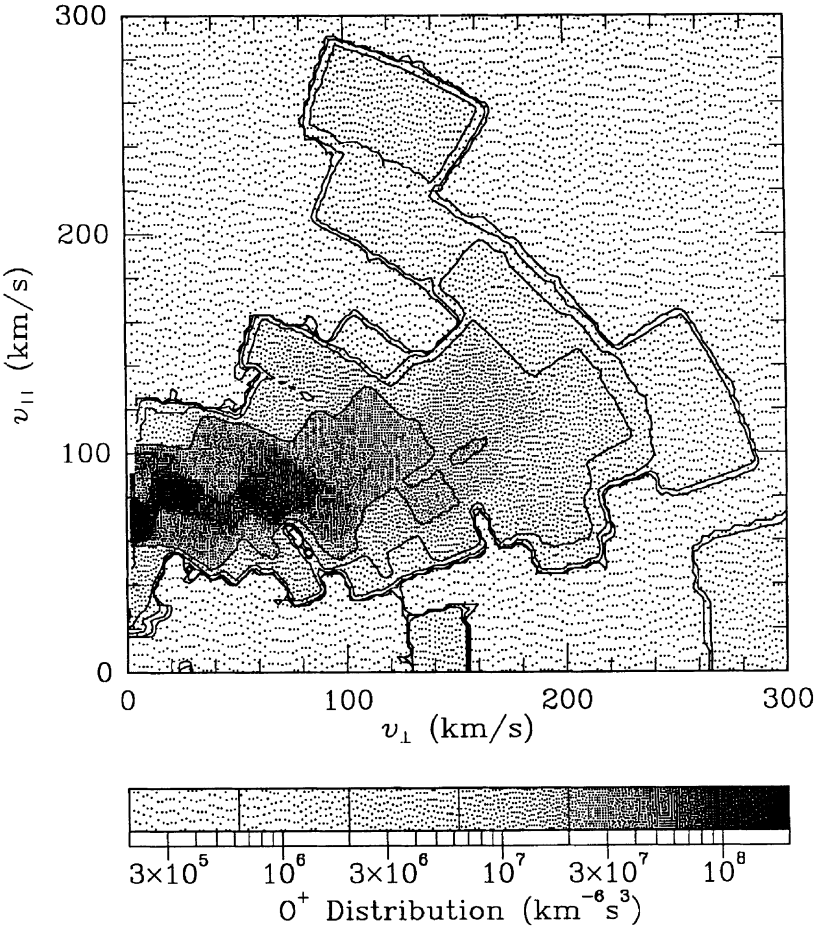

Fig. 9. (*a*) Conic distribution $f_o(v_\perp, v_\parallel)$ constructed from four spins of EICS data near UT 74800 s on day 81288. Contours are placed at half decades, and the darker regions denote the greatest phase space density.

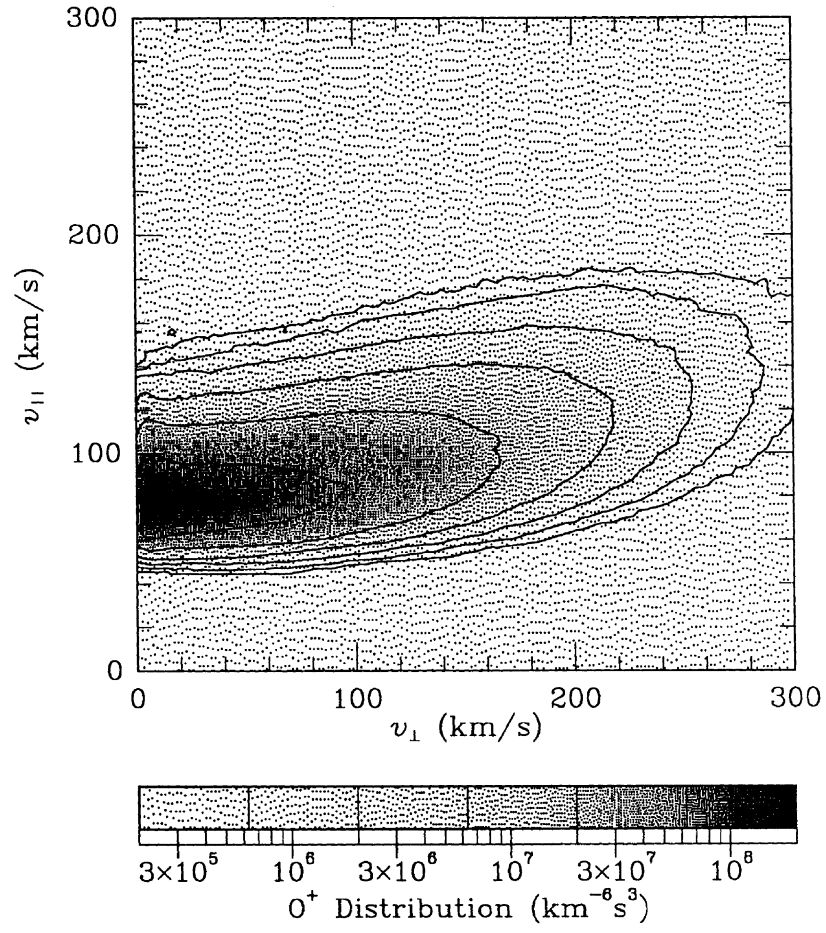

Fig. 9. (*b*) Conic distribution $f_o(v_\perp, v_\parallel)$ constructed from $F(x, y)$ with $\sigma = 8/3$ and a velocity scale of $v_o = 160$ km/s. The contour/halftone representation is identical to that of Figure 9*a*.

a conic with $\sigma = 0$ and $\sigma = 1$, there is little difference between $\sigma = 2$ and $\sigma = 5$. An excellent way to see this is via the path integral results (Figure 8) which show a general insensitivity of the moments to σ values beyond 2.

Another observation to be made from Figure 10*a* is that the error bars for times before UT 74780 s are qualitatively larger than those after this time. One may interpret this as a suggestion from the data that the observed distribution here is far from an "ideal" conic.

Before discussing this ion data further, we present in Figure 10*b* the v_o and σ time series obtained from the PWI data using equations (36) and (24). Because the polarization is undetermined, we have presented v_o values corresponding to a range of $\eta^{1/3}$: 1.0, 0.8, 0.6, and 0.4 for the DC data, and 0.8 and 0.6 for the LFC data. These last two values correspond to between 13% and 5% of the total electric field spectral density being left-hand polarized. We note that the general trend of the event is consistent with Figure 5, and that the DC and LFC data are in general agreement. The DC spectra at this time scale (18 s) are somewhat more dynamic than the LFC data, which have a lower time resolution (32 s). There appears to be some trend for the LFC data to provide somewhat more energetic values of v_o; on the other hand, at these altitudes, the lowest LFC frequency band lies at 1.78 Hz, requiring an extrapolation down to the local oxygen cyclotron frequency. At these time scales, the spectral slope appears to be fairly constant over the displayed interval: $1 \leq \alpha \leq 2$; and it is consistent between DC and LFC.

In comparing particles (Figure 10a) with waves (Figure 10b), we note that the v_o presentations are in reasonable agreement, presenting the same general trend of a climax for the event near UT 74800 s. A value of η in the range $0.2 \lesssim \eta \lesssim 0.5$ would provide reasonably good agreement between the two sets of observations. The situation for σ is perhaps not as conclusive. However, as we remarked above, its determination from the EICS data is not likely to be well constrained, particularly for $\sigma \gtrsim 2$. To some extent the larger values of σ near UT 74800 s may be an aliasing of the increases in v_o at that time. There is, however, a discrepancy between the two v_o plots in the first portion of the time interval.

To examine this discrepancy, we consider the distribution near UT 74730 s. Proceeding as for Figure 9*a*, we average the EICS data from UT 74710–74752 s to obtain the distribution plotted in Figure 11. From this we note the presence of a higher-energy, nonconic component at velocities greater than 140 km/s, which is

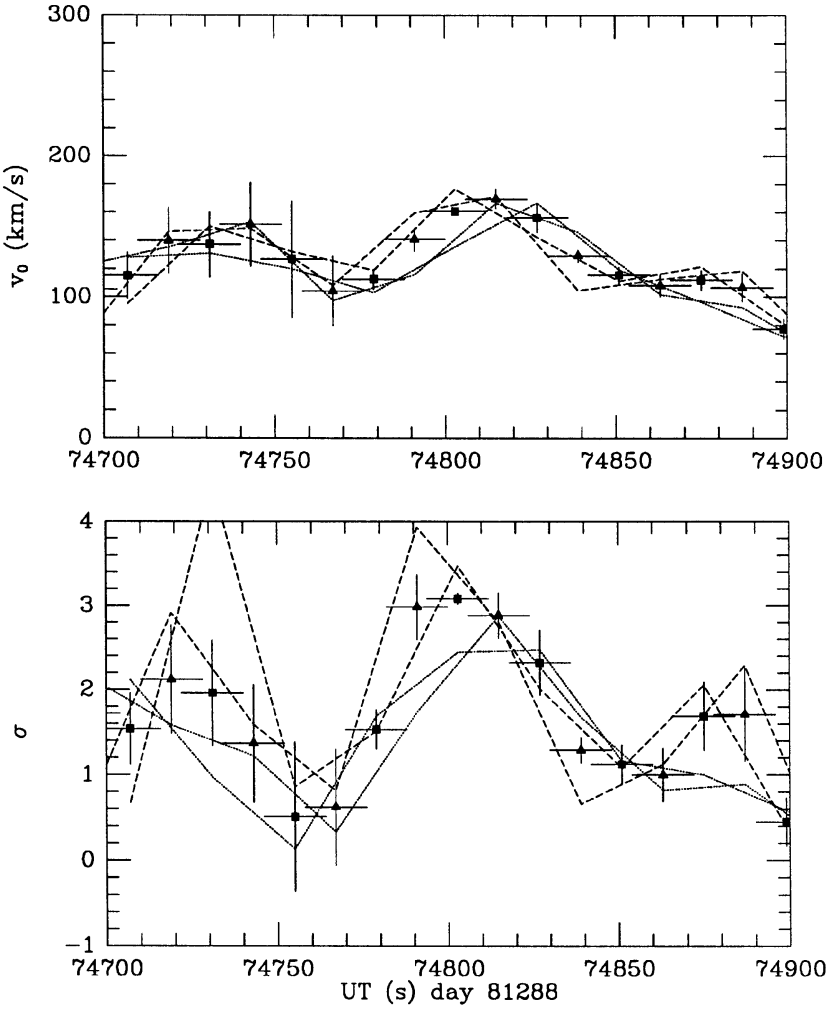

Fig. 10. (*a*) Time series of v_o and σ on day 81288 based on EICS observations. In each panel, the dotted and dashed curves correspond to the right and left halves of the conic, and the solid points with error bars correspond to their average. Squares and triangles distinguish the two ways in which pairs of spins may be composed to construct a complete energy scan; these two ways are undifferentiated for the lines.

sufficiently dense and energetic to corrupt the calculation of the conic moments and hence v_o and σ. Indeed, if we exclude this component from the calculation (roughly 40% of the ions), we obtain $v_o \approx 36 \pm 10$ km/s and $\sigma \approx 1.5 \pm 1$. There still is considerable uncertainty, largely owing to the fact the remaining distribution is largely constructed from the lowest two EICS energy bins; however, the value of v_o is entirely in accord with the range predicted by the PWI instrument.

5.3. Day 82061

We now turn to the second event selected from the EICS data [*Klumpar et al.*, 1984]. Again, we first consider the form of the conic and present an average of three complete energy scans (UT 63799–63841 s) in Figure 12*a*. In comparison with Figure 9*a*, note first of all the lower velocity range of this plot; this is a less energetic event. One consequence is that a significant fraction of the oxygen ions are detected in the lowest-energy ranges of the EICS instrument. Thus the presence of ions at the origin of the plot is probably more an observational (and data reduction) artifact than a discrepancy with the ideal theoretical shape. There is a similar artifact in the apparent acute pitch angle for the peak of the distribution; this is due to the relatively broader energy resolution of the instrument as compared with its angular resolution when mapped to this velocity space.

Computing the moments of this distribution, we find a density $n_i(l_o) \approx 3.3$ cm^{-3}, $v_o \approx 79 \pm 2$ km/s, and $\sigma \approx 2.74 \pm 0.1$. Thus (in round figures) with a velocity scale $v_o = 80$ km/s applied to the numerical solution obtained with $\sigma = 8/3$, we obtain Figure 12*b*. As with the previous event, taking into account the uncertainties, we find reasonably good agreement: a peak near $v_\parallel \sim 40$ km/s as $v_\perp \to 0$, and a comparable $v_\perp$ extent. We see a different observational artifact here in the comb-shaped underside of the distribution in Figure 12*a* which is due to the sampling of alternate energies on consecutive DE-1 spins.

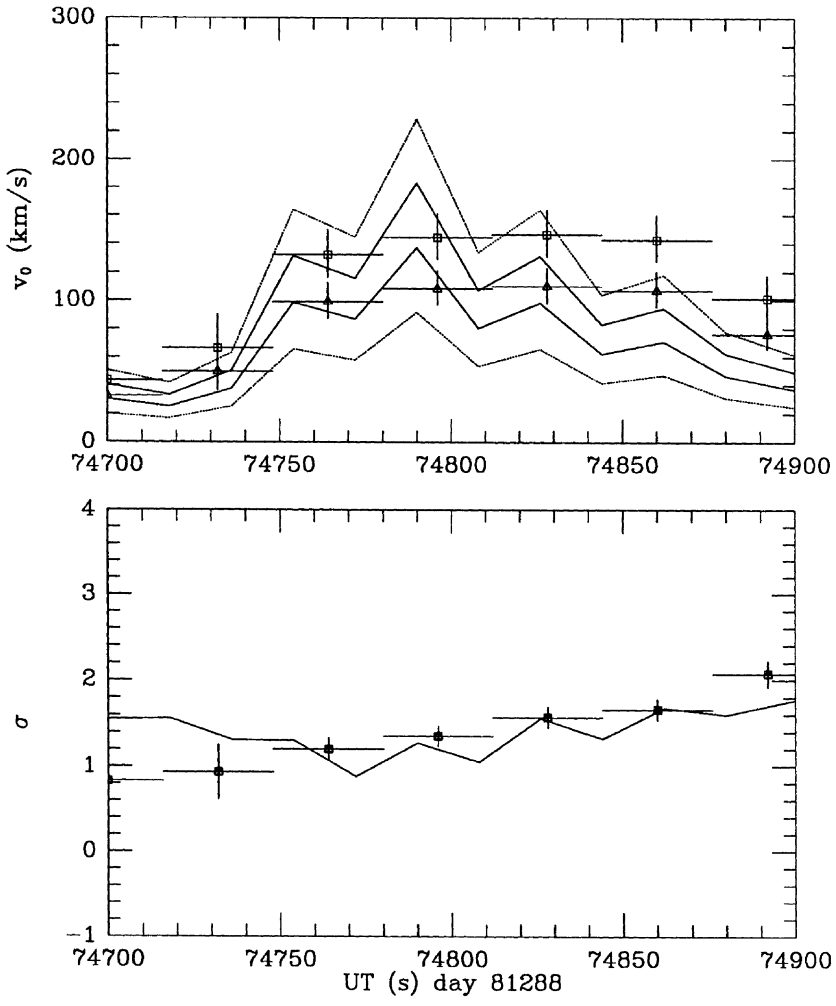

Fig. 10. (*b*) Time series of v_o and σ on day 81288 based on PWI observations. In each panel, the lines correspond to power law fits of the DC data and the open points to power law fits of the LFC data. The multiplicity of v_o values comes from the use of different values of $\eta^{1/3}$: 1.0 (dotted), 0.8 (solid, squares), 0.6 (solid, triangles), 0.4 (dotted).

Turning to the time series of the event, we first present in Figure 13 the result of the spectral analysis of the DC data, in a format identical to that of Figure 5. Comparing Figures 5 and Figure 13, we see that this is a qualitatively less intense event, which is in agreement with the ion data being less energetic.

These remarks hold up when we consider the plots of v_o and σ derived from the two instruments. These are presented in Figure 14*a* for EICS and Figure 14*b* for PWI, in a format analogous to Figures 10*a* and 10*b*. The v_o velocity scale has been reduced to accommodate the less energetic nature of this event. Here again, the EICS v_o values provide a more consistent trend than the σ values; and the greatest σ values/uncertainty corresponds to the peak of v_o. In the PWI data, we find better agreement between LFC and DC spectral intensity than between spectral indices. The spectral index is fairly constant in time; again in the $1 \leq \alpha \leq 2$ range. In comparing the two instruments, we again find a better agreement in v_o values, noting especially the peak for both just prior to UT 63800 s. A value of $\eta^{1/3} \sim 0.6$–0.8 ($0.2 \leq \eta \leq 0.5$) is implied by this agreement. As we have already discussed, we should not take too seriously the apparent discrepancy between the two σ plots.

On the other hand, the wave activity appears to increase towards the end of the interval, yet we do not see this mirrored in the ion data. Again, to investigate this discrepancy we produce the suspect distribution: EICS data from UT 63859–63901 s is plotted in Figure 15. This distribution is considerably farther from being a conic of the similarity-regime type than any we have shown in this paper. One could treat the low-energy portion of the distribution as a contaminant from an unrelated low-energy O^+ population, (i.e., remove the dark wedge at the origin), but this only increases σ and v_o by about 5%, which is not terribly significant. The form of the distribution is also such that such a contamination with a distinct O^+ population is not obvious. On the other hand, the raggedness of the distribution for $v_\perp \sim$ 150 km/s gives us a clue that perhaps there may be some interesting, unresolved temporal effects. Alternatively, it is

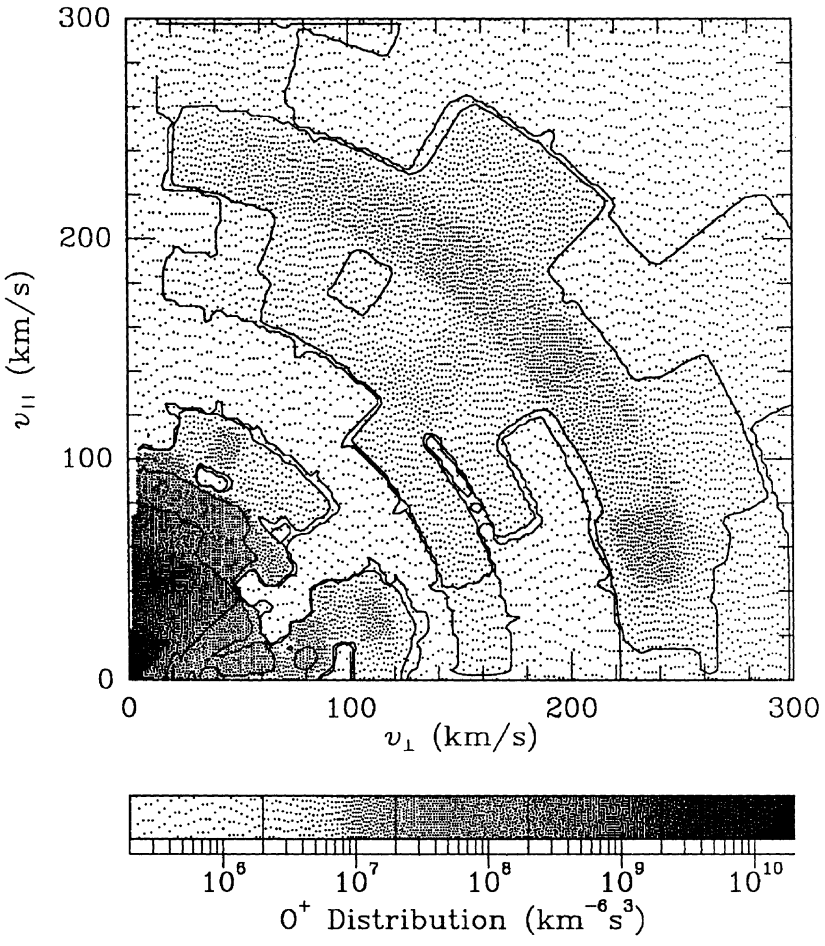

Fig. 11. Conic distribution $f_o(v_\perp, v_\parallel)$ constructed from four spins of EICS data near UT 74730 s on day 81288. The range of phase space densities here is greater than in Figure 9.

possible that at these later times the relative polarization is simply shifting towards a relatively smaller left-hand polarized component ($0.1 \lesssim \eta \lesssim 0.2$).

5.4. Additional Discussion

To summarize the results obtained for these two events, there appears to be a rather clear correlation between the v_o parameter determined separately from EICS and PWI. The situation for σ is not as simple. On the one hand, the agreement appears to be much worse. On the other hand, the disagreement is largely due to the variation of σ as determined from the ion data, and as we have pointed out above, there are a number of reasons not to expect σ to be accurately computed from the ion data. Thus given the agreement for v_o we should be inclined to forgive the σ variation of the ions in an assessment of the validity of the theory as formulated.

Of course, some of the assumptions which we have made in order to constrain the theory and simplify the comparison of the two instruments might be the source of some of the discrepancy. For example, implicit in the assumption that $|E_L|^2 \sim \eta|E_x|^2$ is the assumption that the frequency dependence of $|E_L|^2$ is the same power law as $|E_x|^2$. More generally, we could take $|E_L|^2(f_{ci}) \sim \eta|E_x|^2(f_{ci})$ but assign different spectral indices α_L and α_x to their frequency dependence. Then for the same values of η, it is easy to reconcile $\alpha_L \gtrsim \alpha_x$ with the observations, and it is rather difficult to have $\alpha_L \lesssim \alpha_x$. Since the σ parameter relevant to the conic is $\alpha_L + 1/3$, we would then expect the PWI data to provide a lower bound for the value of σ computed from the EICS data, and this is entirely consistent with the σ plots in Figures 10*a* and 10*b* and Figures 14*a* and 14*b*.

Why this might be the case (i.e., $\alpha_L \neq \alpha_x$) is another question. In the theory, the wave power at higher frequencies is used to provide heating at lower altitudes. Thus in a model for the event where the wave power is generated at high altitudes and is propagating downward, there would be some reflection of the waves which would tend to make the high altitude observations somewhat more energetic than those at lower altitudes. There is even some suggestion (Figure 9 of *Gurnett et al.* [1984]) that the higher frequencies are less energetic at lower altitudes that at higher ones. Thus even if the turbulence was unpolarized, since we construct a model of the turbulence on the flux tube based on the high altitude observations, we must have $\alpha_L \gtrsim \alpha_x$.

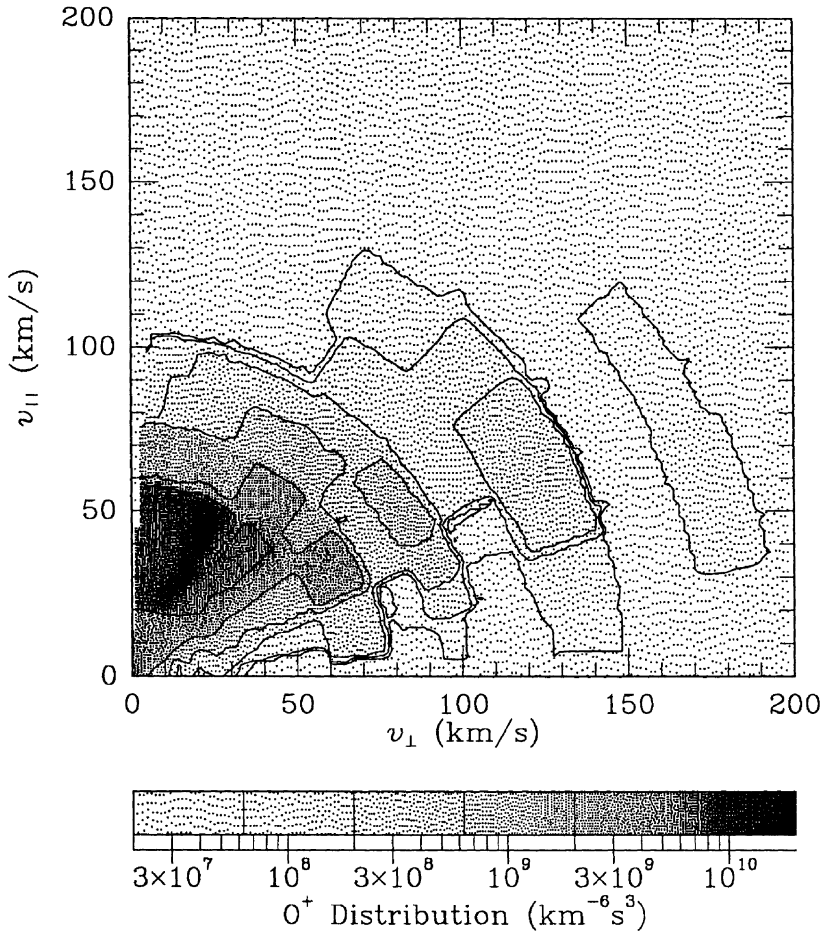

Fig. 12. (*a*) Conic distribution $f_o(v_\perp, v_\parallel)$ constructed from four spins of EICS data near UT 63800 s on day 82061. Contours are placed at half decades, and the darker regions denote the greatest phase space density.

Another significant assumption which affects the analysis is the assumption of a quasi-steady evolution process. As indicated in the general discussion above in section 2, this assumption was made mostly in order to simplify the analysis; but at the same time, observations by a single satellite do not provide sufficient information to include these effects. Qualitatively, we still expect to see conics; quantitatively, we would expect some corrections. For the two events we have presented, the wave activity could be characterized by a temporal turn-on, turn-off sequence. Taking causality into consideration, we would then expect to see the peak of wave activity precede that of the conic energy. Indeed, an allowance of ~ 20 s on day 81288 and of ~ 10 s on day 82061 substantially improves the correlation of the v_o plots in Figures 10*a* and 10*b* and Figures 14*a* and 14*b*.

6. CONCLUSIONS

It should be clear at this point that we have built a strong case for the interpretation of a number of conic events in terms of the ion cyclotron resonance heating mechanism. In this paper we have discussed the theory in considerable detail and approached it at a number of levels. At the lowest level, we discussed a heuristic formulation which includes the basic ingredients of the process and, aside from its pedagogic value, allows for easy "back-of-the-envelope" estimates of the zeroth-order physical effects. At the highest level, we have discussed a similarity transformation which allows a reduction of the process to its high altitude, asymptotic limit which permits a classification of conics bases on exactly two parameters, σ and v_o. Similarly, we discussed three separate events on a number of levels. At the lowest level, we saw that the required wave activity for the generation of conics was present at adequate intensities. At the highest level, we examined the detailed times series along the satellite orbit and found that on a flux tube by flux tube basis, our theoretical framework put the wave and particle data into excellent **quantitative** agreement. We would note that such detailed agreement is rather rarely found in the literature of comparisons of theory with observations, and the only one we know of for the general conic problem.

Given the common occurrence of the required wave turbulence on auroral field lines, and a similar frequency of many conic observations, we would argue that these events are rather typical examples of the formation of conic distributions. Such a class of conics should have a name which reflects our new-found

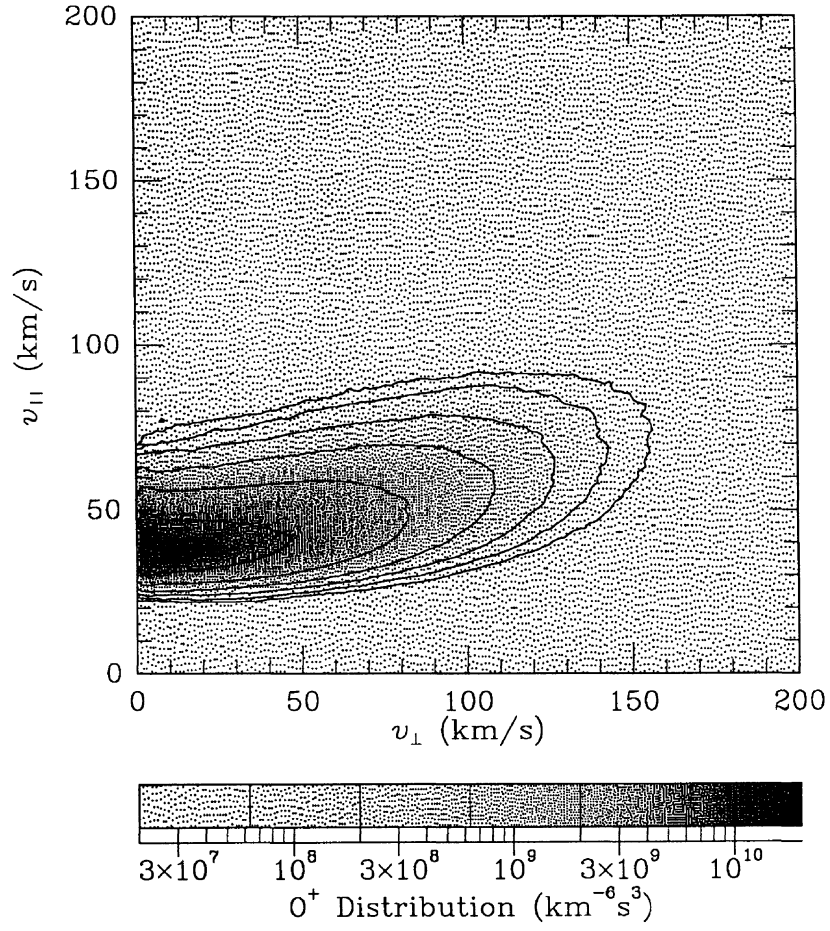

Fig. 12. (*b*) Conic distribution $f_o(v_\perp, v_\parallel)$ constructed from $F(x, y)$ with $\sigma = 8/3$ and a velocity scale of $v_o = 80$ km/s. The contour/halftone representation is identical to that of Figure 12*a*.

understanding of the process; it is appropriate to designate them "ICRH conics," as defined in the introduction, rather than the merely descriptive "bimodal" or "bowl-shaped" conic distributions. This is not to assert, however, that this is the only viable mechanism, or that either all conics or all such conics are manufactured via this mechanism.

Indeed, as indicated in the introduction, quite a number of viable mechanisms were proposed prior to the present work on ICRH conics, and new mechanisms continue to be proposed [*Temerin and Roth*, 1986; *Roth and Temerin*, 1986; *Ball*, 1989]. The point is not that these other mechanisms never work, but rather that there are events where the ICRH mechanism can adequately account for the observations; hence in these events, the other mechanisms are probably limited to effects of higher order. Unfortunately, a determination of this secondary contribution requires even more of the observations than is available for any of the events in the present data set. However, for the events discussed in this paper, it seems likely that such a role is at best secondary: the adequacy of the ICRH mechanism implies that the additional mechanisms would make the conics too energetic; and the additional mechanisms must be consonant with the temporal flow of the events: they must turn on and off with the spectrum of turbulence in the fashion discussed in the preceding section. Additional support for this viewpoint comes from some recent work on cusp conics [*Peterson et al.*, 1989] which showed a likely dominance of the ICRH mechanism over nonresonant heating [*Temerin and Roth*, 1986].

The identification of the events on days 81288, 81318, 82061 as ICRH conics has the obvious corollary that none of the alternate mechanisms often implied by these terms [*Klumpar et al.*, 1984; *Horwitz*, 1986] remain likely candidates for their explication, particularly since the source of the heating is undefined in those treatments. They may be applicable to other conic events, however. This identification is also consistent with the work of *Temerin* [1986], although his ad hoc diffusion model can now be replaced by the ICRH diffusion model.

Turning to the possible presence of a potential drop as suggested by *Klumpar et al.* [1984], we note that the turbulence is still present, so that the ICRH mechanism should still be operative. Thus both the potential drop and the ICRH mechanism will add to the total parallel drift of the conic. If we consider the estimate [*Klumpar et al.*, 1984] that a potential of some 310 V was applied over the last 3,000 km (i.e., $l = 3.8\,R_E$ to $l = l_o = 4.3\,R_E$), then from the scaling (29*b*) with $\sigma = 8/3$ we find

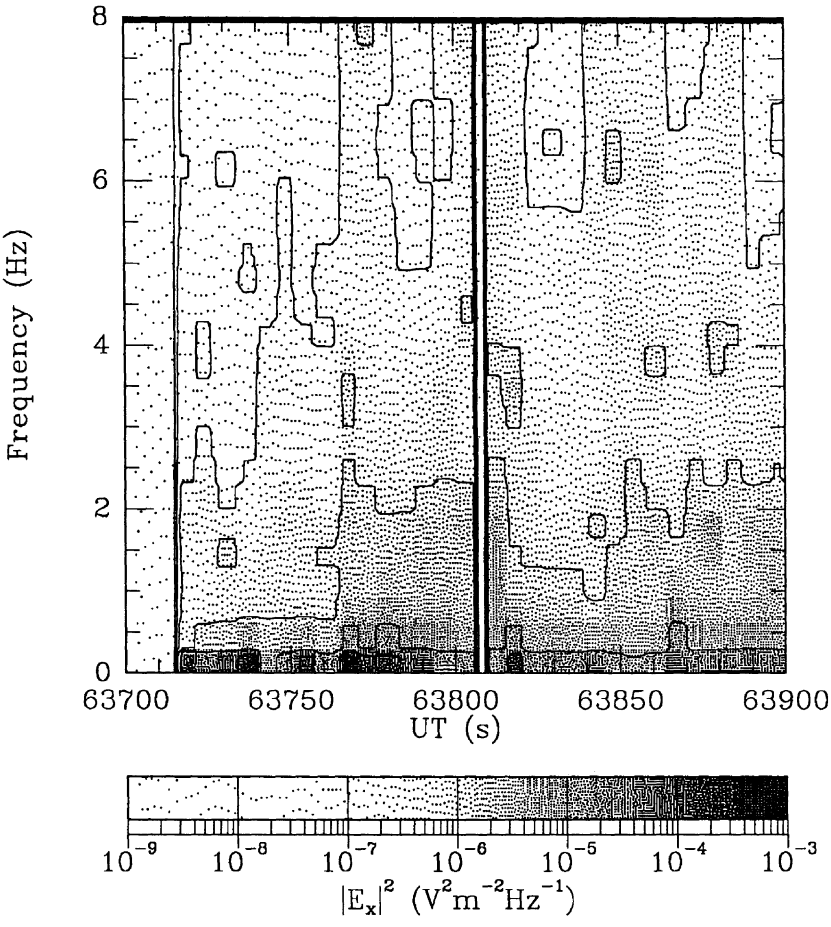

Fig. 13. Electric field spectral density based on the DC data plotted as a function of UT on day 82061. A contour/halftone format is used, where the contours are logarithmically spaced by decades, and the darker regions correspond to the greater spectral density. There is a data gap prior to UT 63750 and near UT 63800 s.

that the conic would have acquired 72% of its mean parallel drift prior to encountering this drop. To make up the remaining drift would require a potential of no more than 24 V, and indeed less, since there would still be a contribution from the ICRH mechanism. One could envision other scenarios, but the main point is inescapable: the same mechanism which provides the perpendicular acceleration also produces a parallel drift, leaving little work for any electrostatic potential. Since the role for the electrostatic potential in the formation of ICRH conics must necessarily be secondary, in the interest of simplicity we have neglected it altogether.

These results should introduce a note of caution into any work which infers a potential drop solely from the parallel drift of ions. That is, as an ICRH conic drifts to altitudes beyond the range of the resonant heating, the effect of the mirror force will be to produce a distribution more akin to a beam than a conic. At some altitude, the finite velocity-space resolution of the instruments makes it impossible to distinguish such a distribution from one generated primarily by acceleration through a field-aligned potential drop of a few hundred volts. Thus one should be somewhat cautious in the interpretation of warm ion beam events. Of course, there are many events where a field-aligned potential can be firmly established [*Collin et al.*, 1986; *Reiff et al.*, 1988]. One should also note that the potential in these latter cases are measured in the thousands of volts.

In addition to these considerations, we note again that most of the assumptions employed in the calculations are also quite secondary to the general viability of the conic generation mechanism. That is, the assumption of a power law frequency dependence for the electric field turbulent spectrum, and a power law dependence of the magnetic field with altitude may readily be relaxed in the presence of more complete information along the flux tube. Unfortunately, such complete information is not likely to ever be available, and it is one of the strengths of the theory that reasonable assumptions obviate the need for this information. A similar unavailability of information would plague efforts to include a realistic time dependence for the flux tube turbulence, rather than the quasi–steady state assumption we have employed in this paper. It is quite likely that some of the discrepancies between the calculations and the observations are indeed due to this missing dependence.

Given the quantitative success of the ICRH conic theory, there is some impetus to return to the wave and particle data sets for a reexamination in the light of the theory. For example, how many

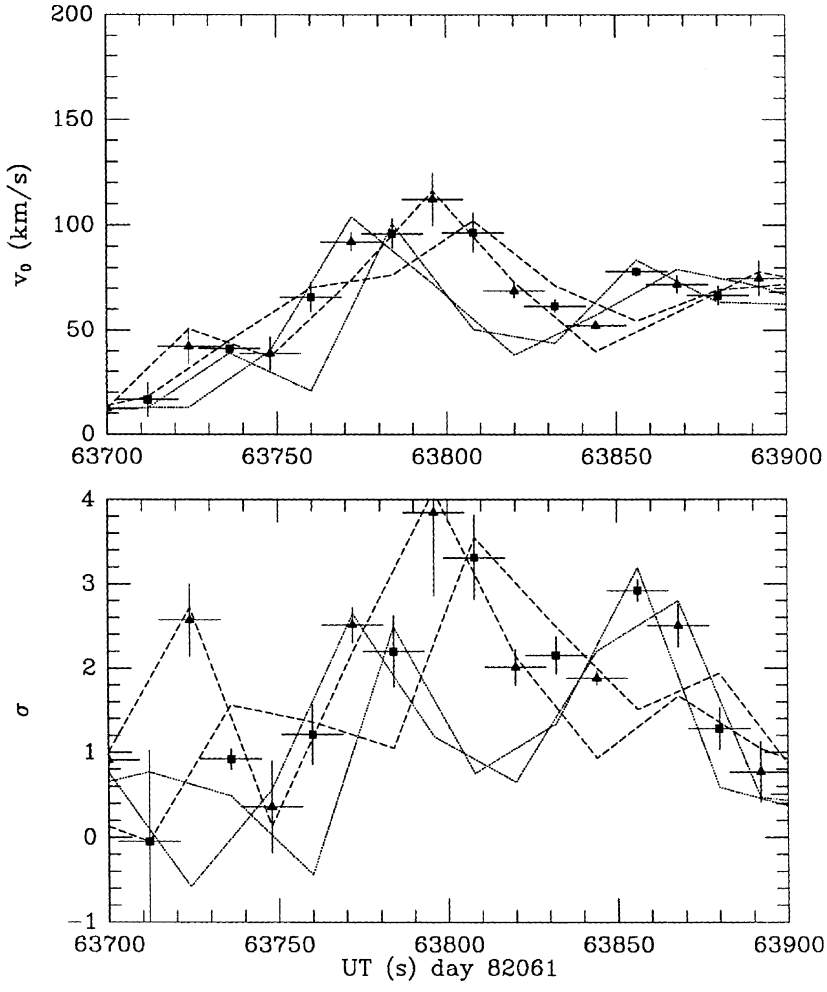

Fig. 14. (*a*) Time series of v_o and σ on day 82061 based on EICS observations. In each panel, the dotted and dashed curves correspond to the right and left halves of the conic, and the solid points with error bars correspond to their average. Squares and triangles distinguish the two ways in which pairs of spins may be composed to construct a complete energy scan; these two ways are undifferentiated for the lines.

of the conics in the EICS surveys [*Yau et al.*, 1984, 1988] are ICRH conics? (Preliminary work suggests that there might be quite a few (*T. Kondo et al.*, Statistical analysis of upflowing ions including hybrid conical pitch angle distributions at DE-1 altitudes, submitted to Journal of Geophysical Research, 1989).) A parallel survey of the low frequency wave data would be invaluable in order to properly address this question. However, the number of events for which all the observational data may be properly analyzed is likely to remain small. For comparison, we note that a search of wave and particle data of an earlier satellite, S3-3, yielded precisely one analyzable event [*Kintner and Gorney*, 1984], for which a definitive interpretation could not be made. That is, neither electrostatic ion cyclotron waves (whose presence could not be unambiguously established) nor lower hybrid waves (present, but not intense) could be held accountable for all of the observed ion energization. Unfortunately, we will never know if the observed ions were O^+, but if some of the observed low-frequency turbulence were electromagnetic, then it appears possible to account for the missing heating. Finally, we note that a recently compiled case study [*Peterson et al.*, 1988] of a DE-1 orbit on January 4, 1984 (day 84004), discussed in detail ~ 20 min of data from one auroral zone crossing. This interval contains two conic events (1439 UT and 1442:30 UT) which are candidates for interpretation as ICRH conics. That is, the O^+ conics appear to have the correct velocity space form, and there is coincident low frequency electromagnetic turbulence present in the LFC of the PWI. Unfortunately, as these are lower altitude events (2.5–3.0 R_E), the bulk of the conic lies in the lowest EICS energy channel, making rather difficult the sort of analysis presented in this paper.

In this paper we have not examined the formation of H^+ conics, both because it is a somewhat more complicated issue and because the formation of the O^+ ICRH conic should proceed independently of effects on the H^+ population. It is more complicated because hydrogen is the dominant species, and it is not at present clear how there can be appreciable power in the

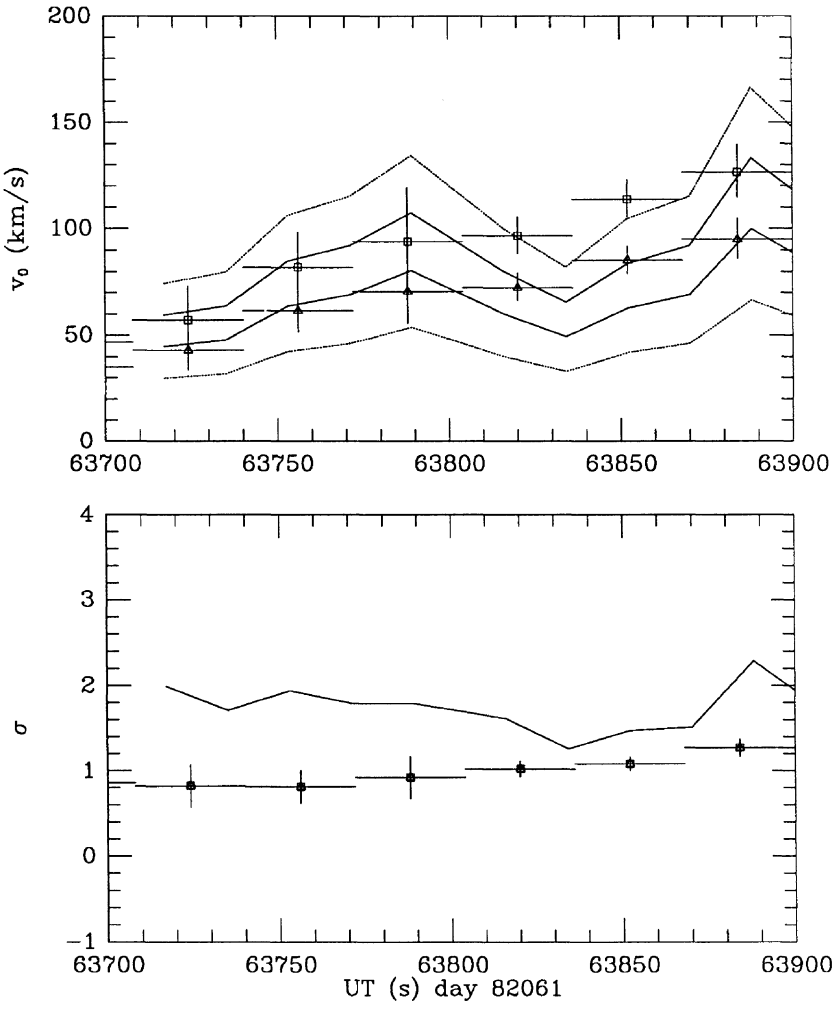

Fig. 14. (*b*) Time series of v_o and σ on day 061 of 1982 based on PWI observations. In each panel, the lines correspond to power law fits of the DC data and the open points to power law fits of the LFC data. The multiplicity of v_o values comes from the use of different values of $\eta^{1/3}$: 1.0 (dotted), 0.8 (solid, squares), 0.6 (solid, triangles), 0.4 (dotted).

left-hand polarization near its cyclotron frequency. Indeed, for the 81318 event, *Chang et al.* [1986] found little power for hydrogen heating, and no H^+ conic was present. On the other hand, Figure 4 is reasonably featureless near the H^+ cyclotron frequency (10 Hz), so any degradation of power in the left-hand polarization must be balanced by an augmentation of the power in the right-hand polarization. The wave observations are similar for the 82061 event. Thus for these higher-altitude events, there may be some H^+ ICRH, but to an extent not easily quantified. Additionally, as is the case for the 81288 event, the presence of a significant magnetospheric high-energy background can also make it difficult to quantify the hydrogen conic. For these reasons we have concentrated the present study on O^+ ICRH conics and leave open the question of H^+ ICRH conics for future study. Such a study would also be in more of a position to investigate the possibility that different heating rates for the two populations might result in a relative drift between H^+ and O^+ which could induce an ion-ion instability leading to a subsequent exchange of energy as has been suggested for auroral ion beams [*Bergmann and Lotko*, 1986; *Roth et al.*, 1989].

As noted in the introduction, conics are frequently observed in the auroral zone. This then raises questions of the correlations of these events with substorms and other magnetospheric activity. And of course, there remains the general question of the source of the turbulence, and its role in magnetosphere–ionosphere coupling. One can perhaps think of closing a loop which includes the generation of the turbulence during a magnetospheric disturbance, the generation of conics in the ionosphere as a result of the turbulence, and the subsequent introduction of ionospheric ions into the magnetosphere via the conics.

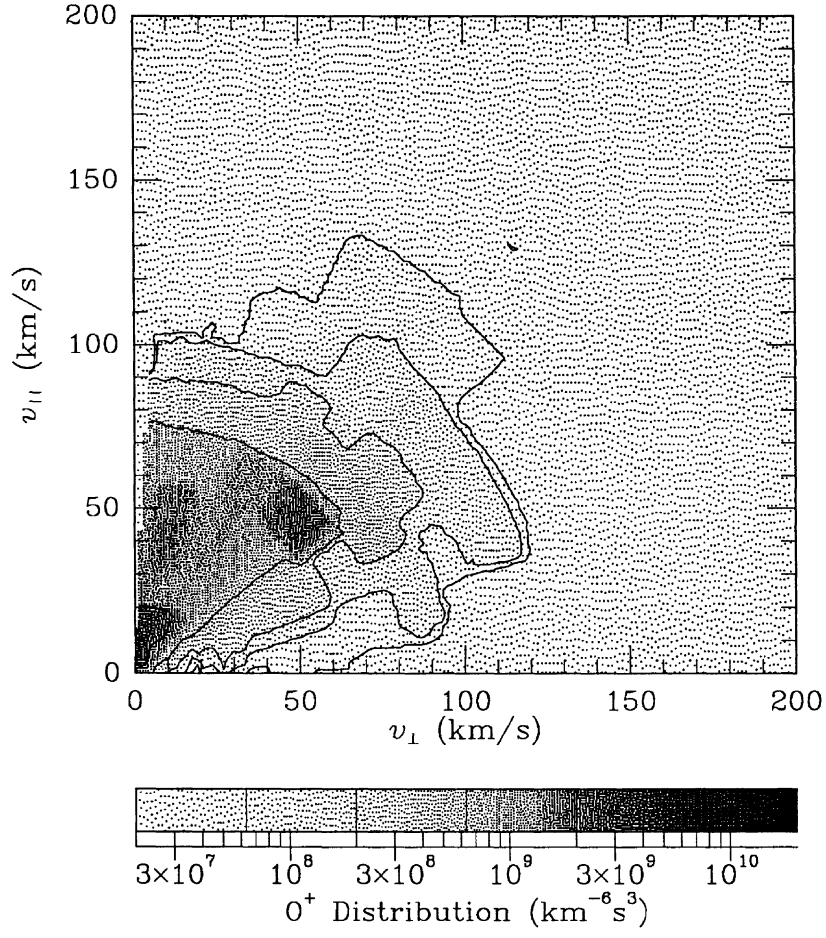

Fig. 15. Conic distribution $f_o(v_\perp, v_\parallel)$ constructed from four spins of EICS data near UT 63880 s. The contour/halftone representation is identical to that of Figure 12*a*.

Acknowledgments. This work has benefited in rather diverse ways from discussions with M. André, J. Burch, H. Collin, J. Jasperse, J. R. Johnson, N. Herskowitz, M. Mellot, P. Reiff, I. Roth, M. Temerin, D. Vvedensky, J. H. Waite, and J. D. Winningham. We also thank the referees for additional stimulating discussion. This work was partially supported by AFGL contract numbers F19628-86-K-0005 and F19628-88-K-0008, and was partially sponsored by the Air Force Office of Scientific Research (AFSC) under contract F49620-86-C-0128 and grant AFOSR-90-0085. The United States Government is authorized to reproduce and distribute reprints for governmental purposes notwithstanding any copyright notation hereon. Additional support from NASA under grant NAGW-1532 and from the M.I.T. Lincoln Laboratory is gratefully acknowledged. The work at Lockheed was supported by NASA contract NAS5-28710.

The Editor thanks J. L. Horwitz and D. Schriver for their assistance in evaluating this paper.

REFERENCES

André, M., H. Koskinen, L. Matson, and R. Erlandson, Local transverse ion energization in and near the polar cusp, *Geophys. Res. Lett., 15*, 107–110, 1988.

Ashour-Abdalla, M., and H. Okuda, Turbulent heating of heavy ions on auroral field lines, *J. Geophys. Res., 89*, 2235–2250, 1984.

Ball, L., Can ion acceleration by double-cyclotron absorption produce O^+ ion conics?, *J. Geophys. Res., 94*, 15257–15264, 1989.

Bergmann, R. A., and W. Lotko, Transition to unstable flow in parallel electric fields, *J. Geophys. Res., 91*, 7033–7045, 1986.

Burch, J. L., Energetic particles and currents: Results from Dynamics Explorer, *Rev. Geophys., 26*, 215–228, 1988.

Burch, J. L., J. D. Winningham, V. A. Blevins, N. Eaker, W. C. Gibson, and R. A. Hoffman, High-altitude plasma instrument for Dynamics Explorer-A, *Space Sci. Instrum., 5*, 455–463, 1981.

Chang, T., and B. Coppi, Lower hybrid acceleration and ion evolution in the suprauroral region, *Geophys. Res. Lett., 8*, 1253–1256, 1981.

Chang, T., G. B. Crew, N. Hershkowitz, J. R. Jasperse, J. M. Retterer, and J. D. Winningham, Transverse acceleration of oxygen ions by electromagnetic ion cyclotron resonance with broad band left-hand polarized waves, *Geophys. Res. Lett., 13*, 636–639, 1986.

Chang, T., G. B. Crew, and J. M. Retterer, Electromagnetic tornadoes in space: Ion conics along auroral field lines generated by lower hybrid waves and electromagnetic turbulence in the ion cyclotron range of frequencies, *Comput. Phys. Commun., 49*, 61–74, 1988.

Cladis, J. B., Parallel acceleration and transport of ions from polar ionosphere to plasma sheet, *Geophys. Res. Lett., 13*, 893–896, 1986.

Coffey, H. E., Geomagnetic and solar data, *J. Geophys. Res., 87*, 926, 1982*a*.

Coffey, H. E., Geomagnetic and solar data, *J. Geophys. Res., 87*, 1733, 1982*b*.

Coffey, H. E., Geomagnetic and solar data, *J. Geophys. Res., 87*, 5310, 1982*c*.

Collin, H. L., E. G. Shelley, A. G. Ghielmetti, and R. D. Sharp, Observations of transverse and parallel acceleration of terrestrial ions at high latitudes, in *Ion Acceleration in the Magnetosphere and Ionosphere, Geophys. Monogr. Ser., vol. 38*, edited by T. Chang, M. K. Hudson, J. R. Jasperse, R. G. Johnson, P.M. Kintner, M. Schulz and G.B. Crew, pp. 67–71, AGU, Washington, D. C., 1986.

Crew, G. B., and T. Chang, Asymptotic theory of ion conic distributions, *Phys. Fluids, 28*, 2382–2394, 1985.

Crew, G. B., and T. Chang, Kinetic treatment of oxygen conic formation in the central plasma sheet by broadband waves, in *Modeling Magnetospheric Plasma, Geophys. Monogr. Ser., vol. 44*, edited by T. Moore and J. H. Waite, pp. 159–163, AGU, Washington, D. C., 1988*a*.

Crew, G. B., and T. Chang, Path integral formulation of ion heating, *Phys. Fluids, 31*, 3425–3439, 1988*b*.

Dusenbury, P. B., and L. R. Lyons, Generation of ion conic distributions by upgoing ionospheric electrons, *J. Geophys. Res., 86*, 7627–7638, 1981.

Fougere, P. F., On the accuracy of spectrum analysis of red noise processes using maximum entropy and periodogram methods: simulation studies and application to geophysical data, *J. Geophys. Res., 90*, 4355–4366, 1985.

Gendrin, R., Wave–particle interactions as an energy transfer mechanism between different particle species, *Space Sci. Rev., 34*, 271–287, 1983.

Goertz, C. K., and R. W. Boswell, Magnetosphere-ionosphere coupling, *J. Geophys. Res., 84*, 7239, 1979.

Gomey, D. J., Y. T. Chiu, and D. R. Croley, Jr., Trapping of ion conics by downward parallel electric fields, *J. Geophys. Res., 90*, 4205–4210, 1985.

Gurnett, D. A., R. L. Huff, J. D. Menietti, J. L. Burch, J. D. Winningham, and S. D. Shawhan, Correlated low-frequency electric and magnetic noise along the auroral field lines, *J. Geophys. Res., 89*, 8971–8986, 1984.

Hasegawa, A., Kinetic properties of Alfvén waves, *Proc. Indian Acad. Sci., 86*, 151, 1977.

Horwitz, J. L., Velocity filter mechanism for ion bowl distributions (bimodal conics), *J. Geophys. Res., 91*, 4513–4523, 1986.

Johnson, J. R., T. Chang, and G. B. Crew, Mode conversion of low frequency waves in a multispecies plasma, *Eos Trans. AGU, 69*, 1374, 1988.

Johnson, J. R., T. Chang, G. B. Crew, and Mats André, Equatorially generated ULF waves as a source for the turbulence associated with ion conics, *Geophys. Res. Lett., 16*, 1469–1462, 1989.

Kennel, C. F., and F. Engelmann, Velocity space diffusion from weak plasma turbulence in a magnetic field, *Phys. Fluids, 9*, 2377, 1966.

Kintner, P. M., and D. J. Gorney, A search for the plasma processes associated with perpendicular ion heating, *J. Geophys. Res., 89*, 937–944, 1984.

Klumpar, D. M., A digest and comprehensive bibliography on transverse auroral ion acceleration, in *Ion Acceleration in the Magnetosphere and Ionosphere, Geophys. Monogr. Ser., vol. 38*, edited by T. Chang, M. K. Hudson, J. R. Jasperse, R. G. Johnson, P.M. Kintner, M. Schulz and G.B. Crew, pp. 389–398, AGU, Washington, D. C., 1986.

Klumpar, D. M., W. K. Peterson, and E. G. Shelley, Direct evidence for two-stage (bimodal) acceleration of ionospheric ions, *J. Geophys. Res., 89*, 10779–10787, 1984.

Lysak, R. L., Ion acceleration by wave–particle interactions, in *Ion Acceleration in the Magnetosphere and Ionosphere, Geophys. Monogr. Ser., vol. 38*, edited by T. Chang, M. K. Hudson, J. R. Jasperse, R. G. Johnson, P. M. Kintner, M. Schulz, and G. B. Crew, pp. 261–270, AGU, Washington, D. C., 1986.

Lysak, R. L., and C. T. Dum, Dynamics of magnetosphere-ionosphere coupling including turbulent transport, *J. Geophys. Res., 88*, 365–380, 1983.

Lysak, R. L., M. K. Hudson, and M. Temerin, Ion heating by strong electrostatic ion cyclotron turbulence, *J. Geophys. Res., 85*, 678–686, 1980.

Papadopoulos, K., J. D. Gaffey, and P. J. Palmadesso, Stochastic acceleration of large M/Q ions by hydrogen cyclotron waves in the magnetosphere, *Geophys. Res. Lett., 7*, 1014–1017, 1980.

Perkins, F. W., ICRF Heating theory, *IEEE Trans. Plasma Sci., PS-12*, 53, 1984.

Peterson, W. K., J. P. Doering, T. A. Potemra, R. W. McEntire, and C. O. Bostrom, Conjugate photoelectron fluxes observed on Atmosphere Explorer C, *Geophys. Res. Lett., 4*, 109–112, 1977.

Peterson, W. K., E. G. Shelley, S. A. Boardson, D. A. Gurnett, B. G. Ledley, M. Sugiura, T. E. Moore, and J. H. Waite, Transverse ion energization and low-frequency plasma waves in the mid-altitude auroral zone: A case study, *J. Geophys. Res., 93*, 11405–11428, 1988.

Peterson, W. K., M. André, G. B. Crew, A. M. Persoon, M. J. Engebretson, C. J. Pollock, and M. Temerin, Heating of thermal ions near the equatorward boundary of the mid-altitude polar cleft, in *Electromagnetic Coupling in the Polar Clefts and Caps, NATO ASI Ser. C: Math. and Phys. Sci., vol. 278*, edited by P. E. Sandhold and A. Egeland, pp. 103–113, Kluwer Academic Publishers, Dordrecht, 1989.

Press, W. H., B. P. Flannery, S. A. Teukolsky, and W. T. Vetterling, *Numerical Recipes*, p. 430, Cambridge University Press, New York, 1986.

Reiff, P. H., H. L. Collin, J. D. Craven, J. L. Burch, J. D. Winningham, E. G. Shelley, L. A. Frank, and M. A. Friedman, Determination of auroral electrostatic potentials using high- and low-altitude particle distributions, *J. Geophys. Res., 93*, 7441–7465, 1988.

Retterer, J. M., T. Chang, and J. R. Jasperse, Ion acceleration in the suprauroral region: A Monte Carlo model, *Geophys. Res. Lett., 10*, 583–586, 1983.

Retterer, J. M., T. Chang, and J. R. Jasperse, Ion acceleration by lower hybrid waves in the suprauroral region, *J. Geophys. Res., 91*, 1609–1618, 1986.

Retterer, J. M., T. Chang, G. B. Crew, J. R. Jasperse, and J. D. Winningham, Monte Carlo modeling of ionospheric oxygen acceleration by cyclotron resonance with broad-band electromagnetic turbulence, *Phys. Rev. Lett., 59*, 148–151, 1987*a*.

Retterer, J. M., T. Chang, G. B. Crew, J. R. Jasperse, and J. D. Winningham, Monte Carlo modeling of oxygen ion conic acceleration by cyclotron resonance with broadband electromagnetic turbulence, in *Physics of Space Plasmas (1985–7), SPI Conference Proceedings and Reprint Series, no. 6*, edited by T. Chang, J. Belcher, J. R. Jasperse and G. B. Crew, pp. 97–111, Scientific Publishers, Inc., Cambridge, Mass., 1987*b*.

Roth, I., and M. K. Hudson, Lower hybrid heating of ionospheric ions due to ion ring distributions in the cusp, *J. Geophys. Res., 90*, 4191–4203, 1985.

Roth, I., and M. Temerin, Nonlinear ion heating in magnetized plasma by magnetized monochromatic low-frequency waves, *IEEE Trans. Plasma Sci., PS-14*, 910–914, 1986.

Roth, I., M. K. Hudson, and R. Bergmann, Effects of ion two-stream instability on auroral heating, *J. Geophys. Res., 94*, 348–358, 1989.

Sagdeev, R. Z., and A. A. Galeev, *Nonlinear Plasma Theory*, pp. 54–55, W.A. Benjamin, New York, 1969.

Sharp, R. D., R. G. Johnson, and E. G. Shelley, Observation of an ionospheric acceleration mechanism producing energetic (keV) ions primarily normal to the geomagnetic field direction, *J. Geophys. Res., 82*, 3324–3328, 1977.

Shawhan, S. D., D. A. Gurnett, D. L. Odem, R. A. Helliwell, and C. G. Park, The plasma wave and quasi-static electric field instrument (PWI) for Dynamics Explorer-A, *Space Sci. Instrum., 5*, 535–550, 1981.

Shelley, E. G., D. A. Simpson, T. C. Sanders, E. Hertzberg, H. Balsiger, and A. Ghielmetti, The energetic ion composition spectrometer (EICS) for the Dynamics Explorer-A, *Space Sci. Instrum., 5*, 443–454, 1981.

Singh, N., and K. S. Hwang, Perpendicular ion heating effects on the refilling of the outer plasmasphere, *J. Geophys. Res., 92*, 13513–13521, 1987.

Singh, N., and R. W. Schunk, Energization of ions in the auroral plasma by broadband waves, *J. Geophys. Res., 89*, 5538–5546, 1984.

Singh, N., R. W. Schunk, and J. J. Sojka, Energization of ionospheric ions by electrostatic hydrogen waves, *Geophys. Res. Lett., 8*, 1249, 1981.

Stix, T. H., *The Theory of Plasma Waves*, McGraw-Hill, New York, 1962.

Temerin, M., Evidence for a large bulk ion conic heating region , *Geophys. Res. Lett., 13*, 1059–1062, 1986.

Temerin, M., and I. Roth, Ion heating by waves with frequencies below the ion gyrofrequency, *Geophys. Res. Lett., 13*, 1109–1112, 1986.

Ungstrup, E., D. M. Klumpar, and W. J. Heikkila, Heating of ions to superthermal energies in the topside ionosphere by electrostatic ion cyclotron waves, *J. Geophys. Res., 84*, 4289–4296, 1979.

Winningham, J. D., and J. Burch, Observation of large scale ion conic generation with DE-1, in *Physics of Space Plasmas (1982–4), SPI Conference Proceedings and Reprint Series, no. 5*, edited by J. Belcher,

H. Bridge, T. Chang, B. Coppi, and J. R. Jasperse, pp. 137–158, Scientific Publishers, Inc., Cambridge, Mass., 1984.

Yau, A. W., B. A. Whalen, W. K. Peterson, and E. G. Shelley, Distribution of upflowing ionospheric ions in the high-altitude polar cap and auroral ionosphere, *J. Geophys. Res.*, *89*, 5507–5522, 1984.

Yau, A. W., W. K. Peterson, and E. G. Shelley, Quantitative parametrization of energetic ionospheric ion outflow, in *Modeling Magnetospheric Plasma, Geophys. Monogr. Ser., vol. 44*, edited by T. E. Moore and J. H. Waite, Jr., pp. 211–217, AGU, Washington, D. C., 1988.

G. B. Crew, T. Chang, and J. M. Retterer, MIT Center for Space Research, Cambridge, MA 02139.

D. A. Gurnett and R. L. Huff, Department of Physics and Astronomy, University of Iowa, Iowa City, IA 52242.

W. K. Peterson, Lockheed Palo Alto Research Laboratory, 3251 Hanover St., Palo Alto, CA 94304.

(Received May 4, 1989;
revised September 15, 1989;
accepted October 13, 1989.)